RSC Advances

PAPER

View Article Online
View Journal | View Issue

Cite this: *RSC Adv.*, 2026, **16**, 28987

From biomass to bioactivity: *Butea monosperma* bark-derived carbon quantum dots for benzopyran synthesis and their *in silico* studies

Sunita Teli, [a] Shivani Soni, [a] Nisarg Rana,[b] Anu Manhas [b] and Shikha Agarwal *[a]

Carbon quantum dots represent a new class of green nanomaterials with exceptional catalytic efficiency and excellent biocompatibility. In this study, a sustainable and green synthetic protocol has been developed using biomass-derived carbon quantum dots obtained from *Butea monosperma* bark as a green nanocatalyst. The catalyst was comprehensively analyzed using HRTEM, SAED, EDX, FT-IR, XRD, UV-visible, and fluorescence spectroscopy, confirming its amorphous nature, surface functionalization, and optical properties, with an average particle diameter of 5.78 nm. The catalyst was successfully utilized for the preparation of a diverse library of benzopyran derivatives *via* the reaction of substituted salicylaldehydes with various C–H activated compounds. The reactions were carried out under mild conditions using EtOH/H_2O (1 : 1) solvent system at room temperature. A diverse library of 17 benzopyran derivatives was synthesized in excellent yields (83–97%) within short reaction times (10–35 min). The catalyst showed remarkable tolerance toward both electron-withdrawing and electron-donating substituents, demonstrating its broad substrate scope and selectivity. The catalyst exhibited excellent recyclability for up to seven consecutive cycles with minimal loss of catalytic activity and favourable green chemistry metrics. Furthermore, *in silico* studies were conducted to evaluate the biological potential of the synthesized compounds against neuropeptide Y5 receptor antagonists, kinase inhibition, and testosterone 17β-dehydrogenase ($NADP^+$). Among them, compounds **3j**, **3i**, and **3q** showed the most promising binding affinities with docking scores of −18.91, −14.35, and −19.49 kcal mol^{-1}, respectively. Key features of the developed protocol include novel source of biomass utilization, metal-free catalysis, operational simplicity, ambient reaction conditions, recyclability and high sustainability.

Received 3rd April 2026
Accepted 18th May 2026

DOI: 10.1039/d6ra02823c

rsc.li/rsc-advances

1. Introduction

The search for sustainable and eco-benign chemical processes has become a central theme in modern synthetic chemistry. The growing demand for cleaner reactions, reusable catalysts, and renewable raw materials has encouraged chemists to rethink traditional synthetic strategies and explore alternative, nature-inspired solutions. In this direction, the integration of green nanomaterials with organic synthesis has emerged as a valuable protocol to achieve efficiency and sustainability in chemical transformations. Among various nanomaterials, carbon quantum dots (CQDs) have recently attracted exceptional interest due to their small size, non-toxicity, large surface area, rich surface chemistry, and excellent aqueous dispersibility.[1] Unlike conventional carbon materials, CQDs possess abundant surface functionalities like alcohol, carboxylic acid, epoxy and amines, which enable strong interactions with organic substrates and make them effective metal-free nanocatalysts.[1–3] In addition to their well-known optical and sensing applications, CQDs have shown promising catalytic behavior in promoting organic reactions under mild conditions.[4]

In recent years, the focus has shifted toward the synthesis of CQDs from biomass-derived precursors, driven by green chemistry principles and circular economy. Biomass materials are renewable, low-cost, and widely available, and they often introduce natural heteroatoms and functional groups into the CQD framework. Various natural sources like fruit peels, leaves, agricultural waste, and flowers have already been explored for this purpose.[5] Many of the reported CQD-based catalytic systems are derived from conventional biomass sources and their complex modifications, and often suffer from limitations such as longer reaction times, harsh reaction conditions, limited substrate applicability, or tedious catalyst recovery processes. In contrast, exploring new biomass resources for developing efficient and sustainable CQD catalysts remains highly desirable. However, the utilization of *Butea monosperma*

[a]*Synthetic Organic Chemistry Laboratory, Department of Chemistry, MLSU, Udaipur-313001, Rajasthan, India*

[b]*Department of Chemistry, School of Energy Technology, Pandit Deendayal Energy University, Gandhinagar, Gujrat-382426, India. E-mail: shikhaagarwal@mlsu.ac.in; sahu70200@gmail.com*

bark as a carbon source for CQD synthesis has not yet been reported. *B. monosperma* is a well-known plant, widely distributed in India and is also known as 'palash' or 'dhak' or 'flame of the forest'. It is abundant in organic constituents, and its bark has been extensively used in traditional medicinal practices.[6] Exploring this material as a carbon precursor not only adds value to biomass waste but also opens new ways for sustainable nanomaterial development.

Beyond synthesis, the application of biomass-derived CQDs as green nanocatalysts in heterocyclic chemistry remains relatively unexplored. Heterocyclic compounds form the backbone of numerous natural products and pharmaceutical agents, and their efficient synthesis continues to be a major focus of organic and medicinal chemistry.[7] Among these, benzopyran derivatives stand out due to their remarkable structural diversity and broad biological importance.[8] Benzopyran consists of a benzene fused with a pyran ring, forming the 4*H*-chromene core. Benzopyran scaffolds are associated with a wide range of pharmacological activities, including antiviral,[9] antifungal,[10] antimicrobial,[11,12] antibacterial,[13] antitubercular,[12] anti-helminthic, anticancer,[14] antioxidant,[9,15] anti-inflammatory,[15] antidiabetic,[16] anticoagulant,[17] anticonvulsant,[18] neurotoxicity,[18] anti-HIV,[19] and antidepressant[20] properties. Fig. 1 illustrates representative biologically active benzopyran-based scaffolds.[21–24] For their synthesis, several methods have been presented in the literature, employing metal catalysts,[25] acids,[26] nanocatalysts,[27] organocatalysts,[24,28] ionic liquids[29] and bio-based catalysts.[30–32] Although many of these methods provide good yields, they often suffer from limitations like long reaction times, elevated reaction temperatures, high catalyst loading, poor recyclability, the requirement of special equipment, *etc*. These drawbacks limit their eco-compatibility and practical applications. Therefore, the development of a mild and eco-friendly catalytic protocol for benzopyran synthesis remains a worthwhile challenge.

Here, we report the green synthesis of *B. monosperma* bark-derived CQDs (BM-CQDs) *via* a hydrothermal approach. The synthesized BM-CQDs were successfully employed as a green catalyst for the preparation of a diverse library of benzopyran derivatives. The catalytic protocol involves the reaction of

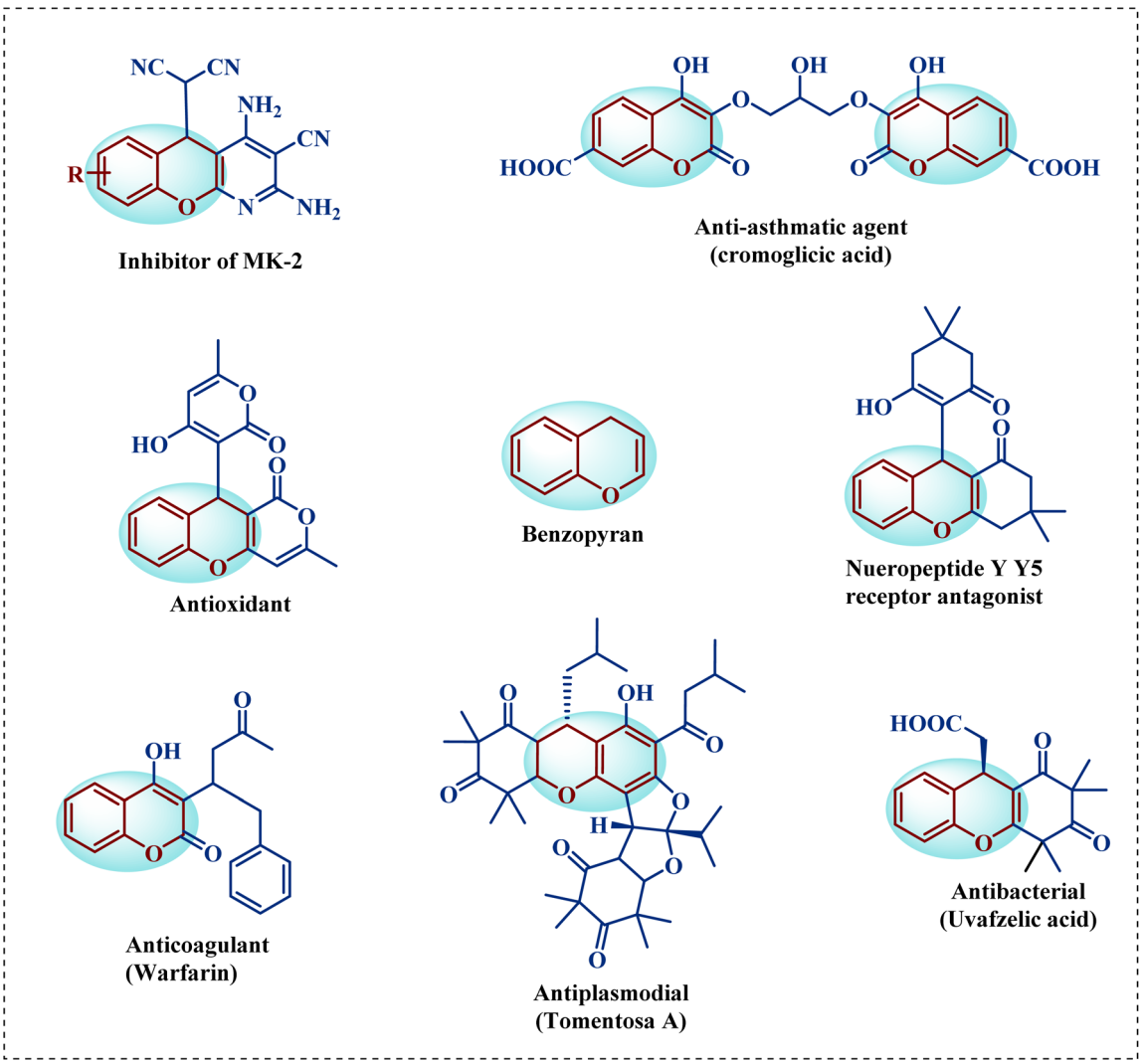

Fig. 1 Biologically important benzopyran-based scaffolds.[21–24]

substituted salicylaldehydes with various C–H activated compounds in different molar ratios (1 : 1, 1 : 2, and 1 : 3) and carried out at RT. In addition to synthetic efficiency, understanding the biological relevance of synthesized scaffolds is crucial for their future application. Therefore, the biological potential of the synthesized benzopyran derivatives was explored through *in silico* studies. Molecular docking studies were performed against Neuropeptide Y5 (NPY5) receptor antagonists, kinase inhibition, and testosterone 17β-dehydrogenase ($NADP^+$). To the best of our knowledge, the biological activity prediction and docking evaluation of benzopyran derivatives against these selected targets have been carried out for the first time, adding a significant novelty to this study. Overall, this work presents a coherent combination of biomass valorization, green nanocatalysis, heterocyclic synthesis, and computational biology.

2. Result and discussion

2.1. Catalyst characterization

In this study, the bark of *B. monosperma* was utilized as a sustainable and new carbon source for the preparation of BM-CQDs through a hydrothermal method. The resulting CQDs were systematically characterized using HRTEM, SAED, EDX, FT-IR, XRD, UV-visible and fluorescence spectroscopy, to determine their structural and optical properties.

The morphology of the synthesized BM-CQDs was examined using HRTEM. The micrographs (Fig. 2a–d) show that the BM-CQDs are uniformly distributed and exhibit a spherical to quasi-spherical shape with no visible agglomeration.[33,34] The SAED pattern (Fig. 2e) displays a single broad diffraction ring, which can be corresponded to the (002) graphene plane of graphitic carbon.[35] This diffuse ring indicates that the BM-CQDs correspond to a single-phase graphite-like structure, but with very small grain size and low crystallinity, resulting in the broad ring characteristic of amorphous carbon domains. The particle size distribution plot (Fig. 2f) reveals an average particle size of 5.58 nm, calculated using Gaussian fitting in ImageJ (Fiji) software. This narrow particle size further validates the successful formation of BM-CQDs.

EDX analysis was carried out to analyse the elemental composition of the synthesized BM-CQDs (Fig. 3). The quantitative results show that oxygen (47.29%) and carbon (33.71%) are the predominant elements, indicating an oxygen-rich carbon framework with abundant surface oxygenated groups.[36,37] Significant calcium content is also observed, which is likely derived from inorganic residues present in the bark precursor. Minor amounts of potassium and magnesium reflect naturally occurring metal ions from the plant source, while trace silicon is also detected. The high oxygen content (relative to carbon) supports the presence of hydrophilic functional groups (–OH, –COOH) and explains the good aqueous dispersibility and surface reactivity of BM-CQDs, which are beneficial for their catalytic behaviour.

The FT-IR spectrum of BM-CQDs (Fig. 4) revealed the presence of various functional groups. A broad absorption peak at 3266 cm^{-1} corresponded to O–H stretching vibrations, confirming the presence of hydroxyl groups.[33] The prominent band at 1637 cm^{-1} corresponded to C=O stretching (carboxyl groups), while the absorption at 623 cm^{-1} was assigned to O–H bending.[36,38,39] These functional groups enhance the hydrophilic properties of BM-CQDs.

The XRD of BM-CQDs (Fig. 5) displayed two broad diffraction peaks centered at $2\theta = 28.85°$ (002) and $2\theta = 42.05°$ (001).[40,41] The broadness of these peaks indicated a low degree of graphitization, reflecting the amorphous carbon framework typically formed during hydrothermal carbonization process.[42] The crystallite size of the synthesized BM-CQDs was calculated using the Debye–Scherrer equation.[43] Two characteristic diffraction peaks corresponding to the (002) and (001) planes were used for this analysis. The (002) peak appeared at $\theta = 14.425°$ with an FWHM (β) of 13.35°, while the (001) peak was observed at $\theta = 21.025°$ with an FWHM of 11.10°. Using the Debye–Scherrer equation as follows:

$$D = \frac{0.9\lambda}{\beta \cos \theta}$$

where λ represents the wavelength of Cu-Kα source ($\lambda = 1.5406$ Å), β shows full width at half maximum (FWHM) of the diffraction peak and θ is the Bragg angle. The crystallite sizes were calculated to be 0.61 nm for the (002) plane and 0.77 nm for the (001) plane. The average crystallite size of the BM-CQDs was thus determined to be approximately 0.69 nm, which is significantly smaller than the particle size (5.58 nm) obtained by HRTEM. This difference confirms the grain or particle size is generally larger than the crystalline size.

The UV-visible absorption spectrum of BM-CQDs (Fig. 6a) shows a distinct absorption band at 277 nm, characteristic of n–π* transitions of C=O bonds as well as π–π* transitions from C=C aromatic domains.[2,44] These features indicated the presence of conjugated carbon structures along with O-containing functionalities on the surface. The inset images highlighted the transparent yellow-brown colour of BM-CQDs in daylight and their bright fluorescence (green colour) under UV light. The photoluminescence properties of BM-CQDs were analysed using fluorescence spectroscopy (Fig. 6b). The BM-CQDs exhibited a broad emission band spanning 310–650 nm, with a strong maximum centred at 438 nm, identifying it as the optimal emission wavelength.[45,46]

2.2. Catalytic activity

To evaluate the catalytic activity of the BM-CQDs, we selected the reaction between 2-hydroxybenzaldehyde and dimedone (1 : 2 molar ratio) as the model reaction. A detailed optimization study was then carried out by systematically varying the solvent, reaction time, catalyst loading, temperature and other conditions (Table 1).

Initially, control experiments conducted in the absence of any catalyst revealed very slow progress and poor conversions. Without BM-CQDs, the reaction in EtOH, H_2O and EtOH + H_2O (1 : 1) solvent systems delivered only 37%, 35% and 43% yields, respectively in 150 min (entry 1–3; Table 1). Introducing BM-CQDs (0.50 mL) significantly improved the reaction efficiency.

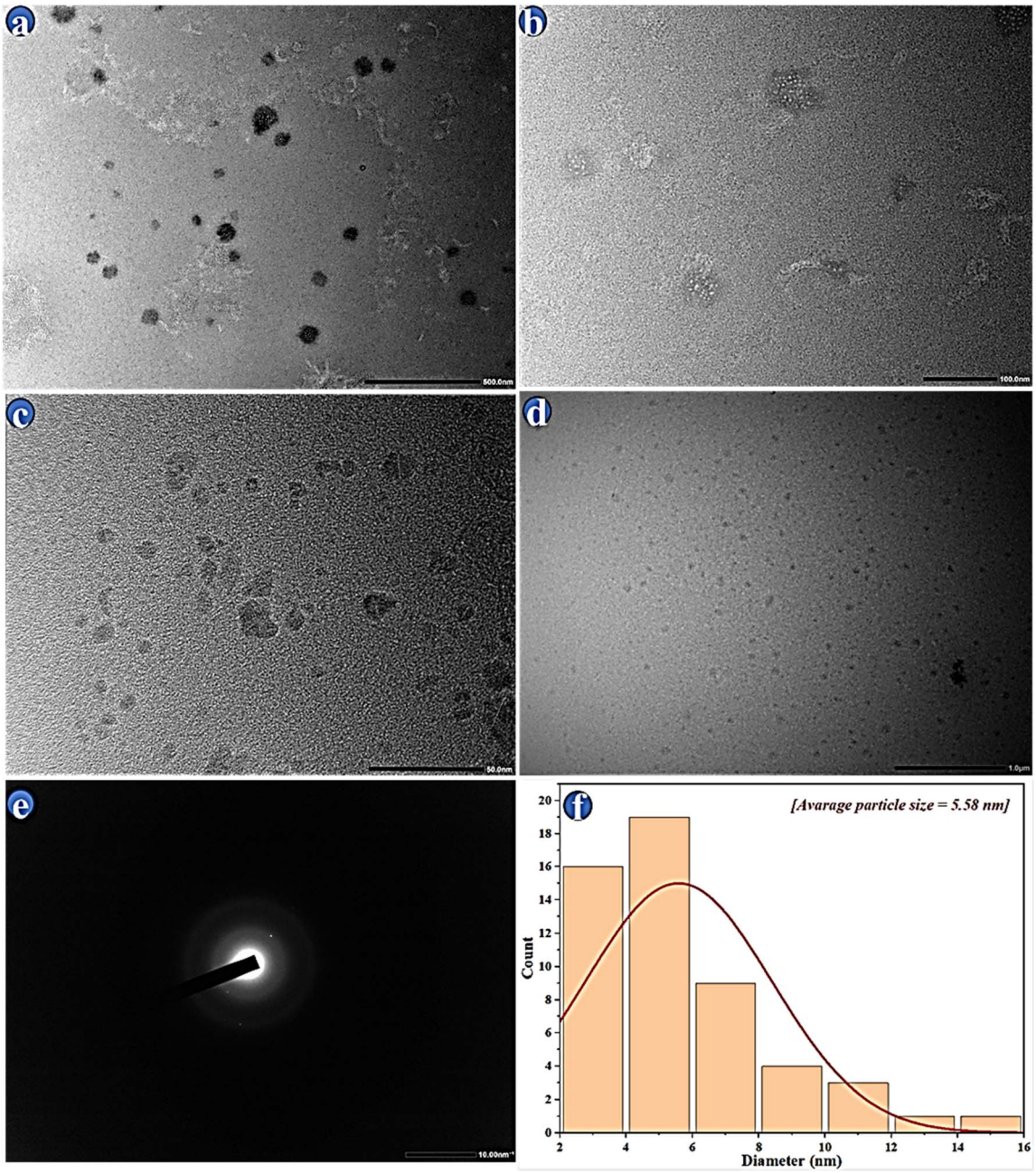

Fig. 2 HRTEM images of BM-CQD at different resolutions: (a) 500 nm, (b) 100 nm, (c) 50 nm, (d) 1 μm, (e) SAED pattern, (f) size distribution histogram of BM-CQD in its 50 nm resolution.

Ethanol alone afforded 94% yield in just 15 min (entry 4; Table 1), whereas pure water yielded 89% (entry 5; Table 1). Notably, the mixed solvent system EtOH/H_2O (1 : 1) emerged as the most effective medium, providing the target compound in an excellent 97% yield within just 15 min at RT (entry 6; Table 1). Changing the solvent ratio to EtOH/H_2O (1 : 2) resulted in a slight decrease to 95% (entry 7; Table 1), confirming the superiority of the 1 : 1 mixture. The influence of catalyst loading was further examined. A reduced quantity of BM-CQDs (0.25 mL) led to 92% yield (entry 8; Table 1), whereas increasing the catalyst loading to 0.75 mL did not provide any benefit by maintaining a 97% of yield (entry 9; Table 1). Thus, 0.50 mL of BM-CQDs was identified as the optimal catalyst amount. The role of solvent was further highlighted by the solvent-free reaction, which afforded only 72% yield in 30 min (entry 10; Table 1). Even when the reaction was performed at 80 °C, the yield remained at same 97% yield (entry 11; Table 1), suggesting that higher temperature does not significantly influence the outcome and that RT conditions are indeed sufficient. An ultrasonic-assisted protocol was also tested, giving 91% yield in 20 min (entry 12; Table 1), but it did not outperform the standard stirring method. Thus, the best conditions for synthesizing

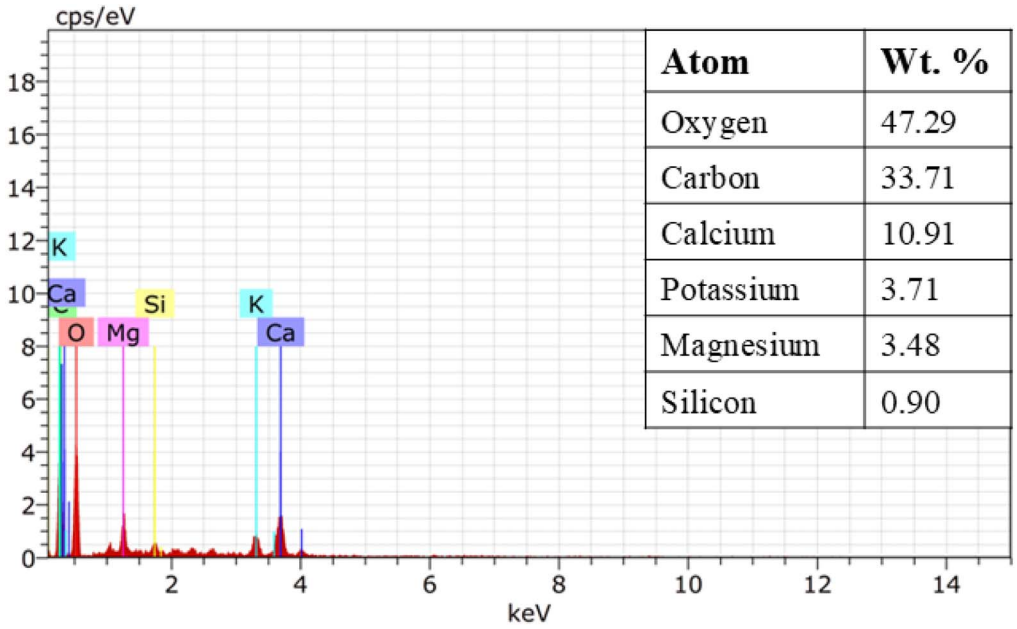

Atom	Wt. %
Oxygen	47.29
Carbon	33.71
Calcium	10.91
Potassium	3.71
Magnesium	3.48
Silicon	0.90

Fig. 3 EDX spectrum of BM-CQDs.

benzopyran series were BM-CQD (0.50 mL) in EtOH/H_2O (1 : 1) at RT, giving 97% yield in just 15 min.

To further assess the catalytic efficiency of BM-CQDs, the present method was compared with previously reported protocols for the synthesis of benzopyran derivatives, as summarized in Fig. 7. Earlier studies employed a wide range of catalysts, including metal-based catalysts (Fe/NaY zeolite[25]), nanocatalysts (nano-$ZnAl_2O_4$ (ref. 27)), organocatalysts (taurine,[24] AcOH,[28] L-proline[47]), biobased catalysts (β-cyclodextrin,[30] lemon extract,[31]), ionic liquids ([$[(CH_2)_4SO_3HMIM][HSO_4]$[29]), solid acid catalysts (cellulose sulfuric acid[26]) *etc.* While several of these methods provide good to excellent yields and utilize green catalytic systems, many still suffer from notable limitations. Common drawbacks include the

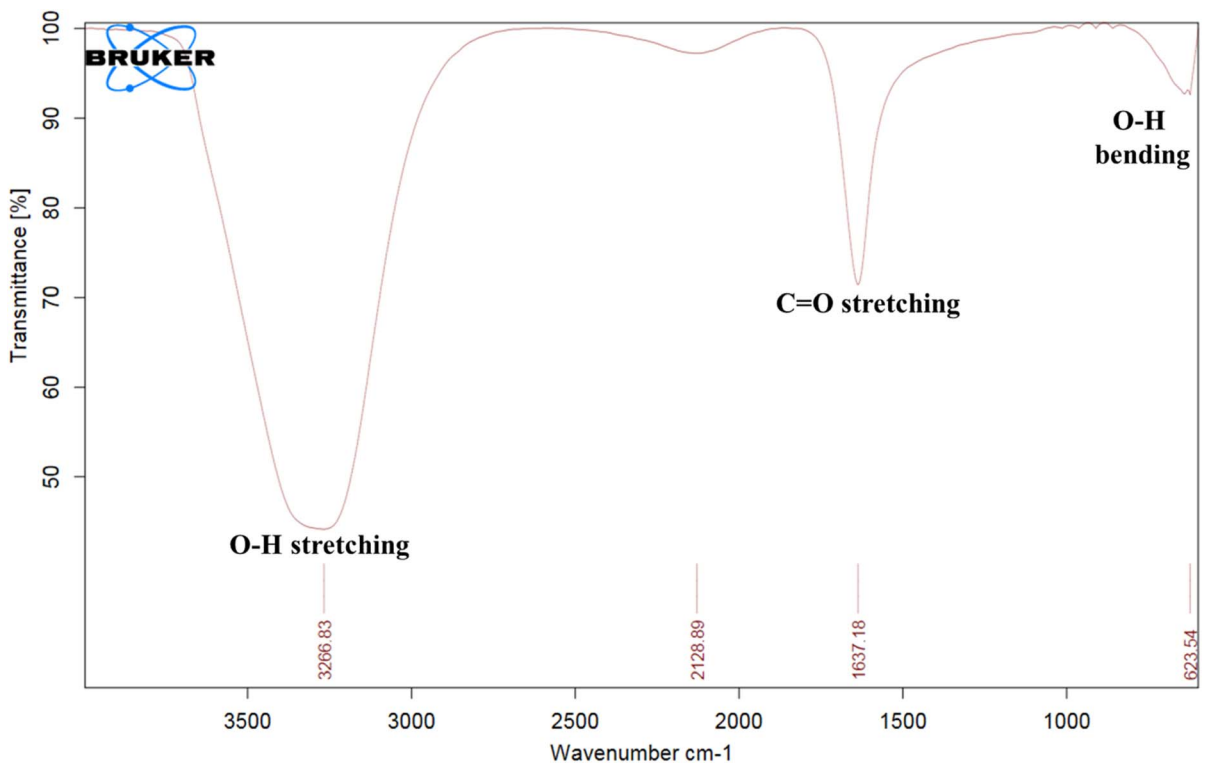

Fig. 4 FTIR spectrum of BM-CQDs.

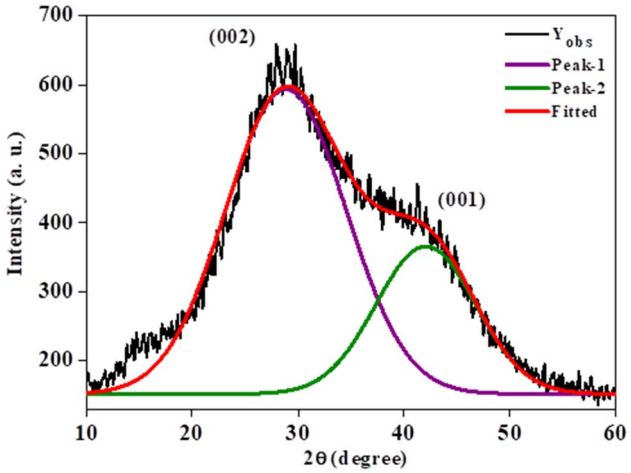

Fig. 5 XRD pattern of BM-CQD.

requirement of long reaction times, elevated temperatures, high catalyst loading, or energy-assisted techniques. In some cases, reactions were proceeded under ambient conditions or even without a catalyst, but these approaches often resulted in reduced efficiency or prolonged reaction durations.[48] Additionally, several protocols involve elevated workup procedures, limiting their practical applicability. In contrast, the present method employing BM-CQDs as a green nanocatalyst effectively addresses these limitations. The reactions completed smoothly under ambient conditions and delivered excellent yields within short reaction times, and do not require special equipment or elaborate purification steps. Additionally, the catalyst loading is also minimal, and the BM-CQDs can be easily recovered and reused without loss of activity. Overall, this comparative study highlights the superiority of BM-CQDs in terms of efficiency, sustainability, operational simplicity, and practical scalability for the preparation of pyran derivatives.

2.3. Synthesis of benzopyrans

A diverse library of benzopyran derivatives was synthesized through the reaction of salicylaldehyde analogues with various CH-activated compounds using different molar ratios (1 : 1, 1 : 2, and 1 : 3), as highlighted in the Scheme 1. To evaluate the substrate scope and functional group tolerance of the developed BM-CQD-catalyzed protocol, both electron-withdrawing and electron-donating groups on the salicylaldehyde framework were explored. Electron-donating substituents included 4-methyl-2-hydroxybenzaldehyde and 2-hydroxy-3-methoxybenzaldehyde, while electron-withdrawing groups such as 2-hydroxy-5-nitrobenzaldehyde, 3-bromo-5-chloro-2-hydroxybenzaldehyde, 5-fluoro-2-hydroxybenzaldehyde, and 4-chloro-2-hydroxybenzaldehyde were also utilized and gave excellent yields. Additionally, polycyclic aromatic systems like 2-hydroxy-1-naphthaldehyde also participated efficiently in the reaction. A broad range of CH-activated compounds were utilized; such as dimedone, 1,3-cyclohexanedione, 4-hydroxy-6-methyl-2*H*-pyran-2-one, 4-hydroxy-2*H*-chromen-2-one, barbituric acid, 3-methyl-1-phenyl-2-pyrazolin-5-one and malononitrile. Under the optimized conditions, a total of 17 benzopyran derivatives were synthesized efficiently, among which three compounds were found to be new (Scheme 2). The structural integrity of the synthesized products was confirmed by detailed ^{1}H NMR, ^{13}C NMR, ^{19}F NMR, and HRMS analyses, and melting point determination (Fig. S1–S44).

From our findings and based on previous reports, plausible mechanistic pathways for the preparation of benzopyran derivatives were proposed, as highlighted in Schemes 3–5. BM-CQDs acted as an efficient green nanocatalyst due to the presence of abundant surface –OH/–COOH functional groups. These groups facilitated hydrogen bonding, activated carbonyl functionalities, promoted tautomerization of active methylene compounds and even stabilized the key intermediates. Initially, salicylaldehyde derivative **1** was activated *via* hydrogen bonding with BM-CQDs, enhancing the electrophilicity of the aldehydic carbon. Simultaneously, C–H activated compounds **2′** underwent tautomerization to its active form **2**. A Knoevenagel

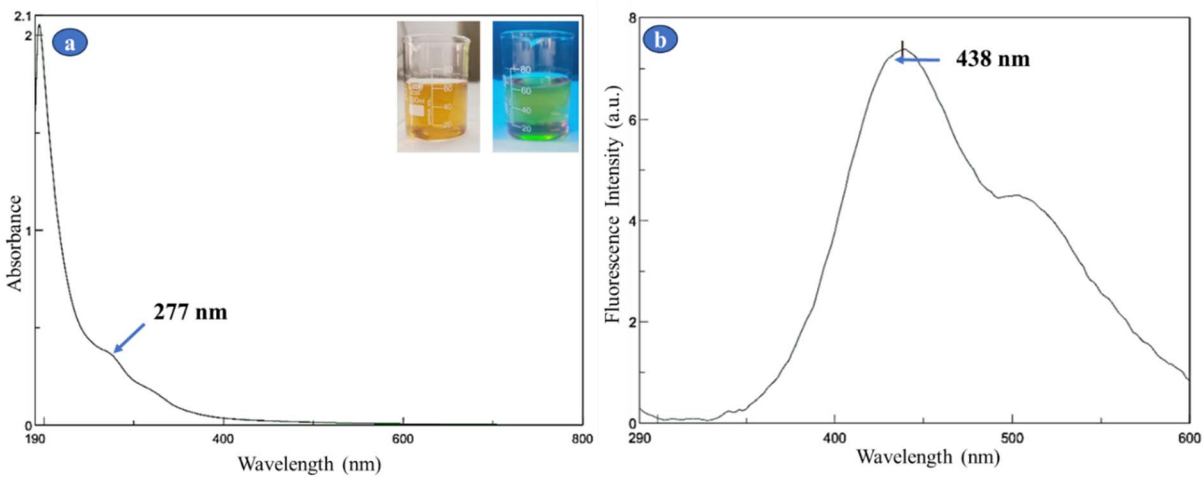

Fig. 6 UV-visible spectrum (a) and fluorescence emission spectrum (b) of BM-CQDs.

Table 1 Exploration of reaction variables for the preparation of benzopyrans[a]

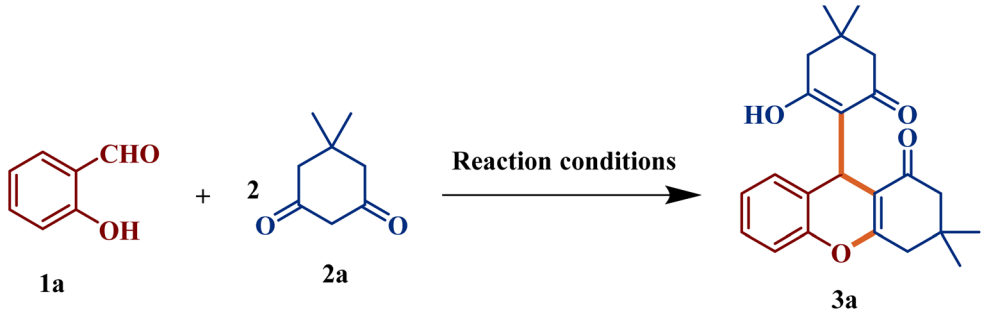

Entry	Catalyst (mL)	Solvent	Temperature	Time (min.)	Yield (%)
1	—	EtOH	RT	150	37
2	—	H_2O	RT	150	34
3	—	EtOH + H_2O (1 : 1)	RT	150	43
4	BM-CQD (0.50)	Ethanol	RT	15	94
5	BM-CQD (0.50)	H_2O	RT	15	89
6	**BM-CQD (0.50)**	**EtOH + H_2O (1 : 1)**	**RT**	**15**	**97**
7	BM-CQD (0.50)	EtOH + H_2O (1 : 2)	RT	15	95
8	BM-CQD (0.25)	EtOH + H_2O (1 : 1)	RT	15	92
9	BM-CQD (0.75)	EtOH + H_2O (1 : 1)	RT	15	97
10	BM-CQD (0.50)	—	RT	30	72
11	BM-CQD (0.50)	EtOH + H_2O (1 : 1)	80 °C	20	97
12	BM-CQD (0.50)	EtOH + H_2O (1 : 1)	RT	20	91[b]

[a] Reaction condition: 0.5 mmol 2-hydroxy benzaldehyde, 1 mmol dimedone and 4 mL solvent. [b] Ultrasonic method was employed.

condensation between **1** and **2** afforded the intermediate (**i**). Subsequent dehydration led to the Knoevenagel adduct (**ii**), which acted as Michael acceptor and underwent for Michael addition with second molecule of CH-activated compound **2** to form intermediate (**iii**). Further intramolecular cyclization produced intermediate (**iv**), which upon dehydration yielded the final benzopyran derivatives **3a–3n** (Scheme 3).[49]

For compounds **3o–3p**, salicylaldehyde **1** reacted with 2-pyrone **2**. Activation of the aldehyde by BM-CQDs promoted Knoevenagel condensation, forming intermediate (**i**). This intermediate underwent dehydration to generate (**ii**), followed by intramolecular cyclization, leading to the cyclic intermediate (**iii**). The reaction proceeded through a ring-opening rearrangement, ultimately giving benzopyran derivatives **3o–3p** (Scheme 4).[50]

In the case of compound **3q**, BM-CQDs simultaneously activate salicylaldehyde **1** and malononitrile **2′**, which underwent tautomerization to **2**. A Knoevenagel condensation between **1** and **2′** yielded intermediate (**i**), which formed intermediate (**ii**) *via* dehydration. This intermediate underwent intramolecular cyclization and gave intermediate (**iii**). Further intermediate (**iii**) converted into intermediate (**iv**) followed by Michael addition with the activated nucleophile (**2**). At last, 3rd mole of malononitrile attacked on the nitrile group of pyran compound (**iv**) and gave intermediate (**v**). Subsequent intramolecular cyclization gave intermediate (**iv**), and dehydration led to the synthesis of the desired derivative **3q** (Scheme 5).[22,51]

2.4. Reusability

The reusability of the BM-CQDs was evaluated to assess their stability and practical applicability. After each reaction cycle, the solid product was removed by simple filtration and the BM-CQDs remained in the ethanol–water filtrate. This filtrate was directly reused for the next cycle without any additional purification steps such as solvent removal, washing, or drying, demonstrating the excellent operational convenience of the catalyst recovery method. The BM-CQDs retained high catalytic efficiency over numerous cycles. As illustrated in Fig. 8, the catalyst maintained outstanding performance for up to seven consecutive runs, with only a minor decline in yield from 97% in the first cycle to 85% in the seventh cycle. The persistent green fluorescence of the recycled BM-CQDs under UV light further indicates that their optical properties remain largely unchanged during reuse, supporting their structural stability. To confirm the preservation of the catalyst's structural features, FT-IR (Fig. 9) and XRD (Fig. 10) analyses were carried out on the reused BM-CQDs. The spectrum and diffraction patterns closely matched those of the freshly synthesized sample, verifying that the fundamental functional groups and amorphous carbon framework remained identical even after repeated catalytic applications. These observations collectively highlight the robustness, recyclability, and durability of BM-CQDs as an efficient green catalyst.

2.5. Gram scale synthesis

To demonstrate the scalability and practical applicability of the developed protocol, a scale-up synthesis of the benzopyran

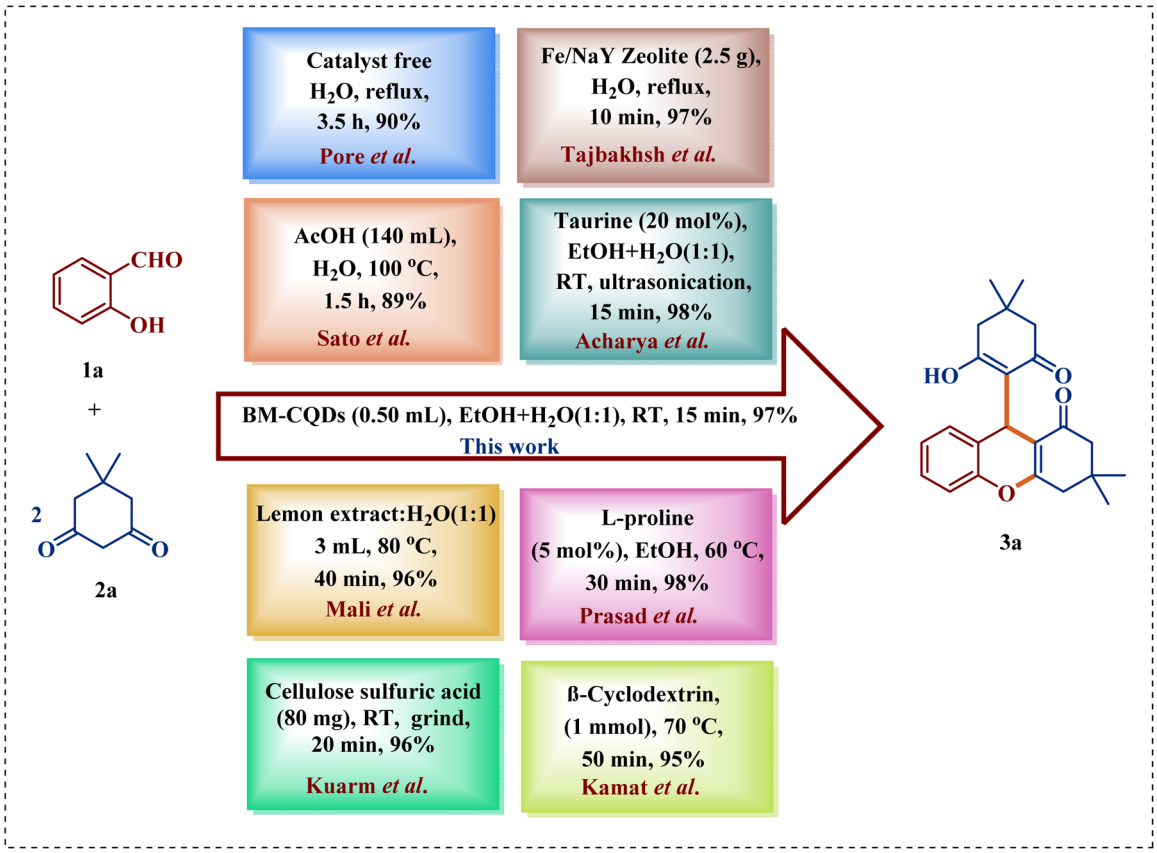

Fig. 7 Comparative study of our work with previously reported methods.[24–26,28,30–32,47,48]

derivative **3a** was proceeded under the optimized reaction conditions (Scheme 6 and Fig. S45). In this experiment, salicylaldehyde (4.0 mmol, 0.425 mL) and dimedone (8.0 mmol, 1.122 g) were combined in the presence of BM-CQDs (0.5 mL) as the catalyst using an ethanol–water solvent system (32 mL). The reaction mixture was stirred at RT and was completed within 25 min, as monitored by TLC. After completion, the product was isolated by simple filtration, washed with water, and dried to give 1.381 g of the benzopyran derivative in an excellent 94% isolated yield. This gram-scale experiment confirms the robustness, efficiency, and scalability of the BM-CQD-catalyzed protocol for the preparation of benzopyran derivatives.

2.6. Green chemistry metrics

Green chemistry focuses on designing chemical processes that minimize waste generation, reduce the use of hazardous substances, and improve overall sustainability without compromising efficiency.[52] To quantitatively assess how environmentally benign a synthetic protocol is, green chemistry metrics (GCM) such as atom economy (AE), reaction mass efficiency (RME), *E*-factor, process mass intensity (PMI), and eco-score are widely employed.[53] These metrics provide a clear, numerical insight into material utilization, waste generation, and the overall environmental footprint of a reaction, making them essential tools for comparing and validating modern sustainable synthetic methodologies. In this context, the greenness of the BM-CQD-catalyzed synthesis of benzopyran derivatives was systematically evaluated using the above metrics, and the results are highlighted in Fig. 11 and Table S1. The reactions consistently exhibited high atom economy (89.60–95.14%), reflecting efficient incorporation of reactant atoms into the desired products with minimal by-product generation. Similarly, the RME values (76.64–88.06%) indicate excellent material utilization, further highlighting the effectiveness of this one-pot developed procedure. The low *E*-factor values (0.136–0.305) and PMI values (1.156–1.324) demonstrate minimal waste formation and reduced material input, which are key indicators of an eco-benign method. The high eco-score values (81.37–88.36) across the diverse compound library confirm the overall green and sustainable nature of the protocol. Collectively, these results validate that the protocol aligns well with the principles of green chemistry and offers a sustainable alternative to conventional benzopyran synthesis methods, making it attractive for both academic research and potential scale-up applications.

2.7. Molecular docking

2.7.1. Activity prediction. To obtain preliminary information about the possible biological activities of the synthesized benzopyran derivatives, PASS online software[54] was used for activity prediction. The analysis was carried out by evaluating each compound against multiple biological activities, but predictions with a probability of activity (Pa) value above 0.5 were considered biologically significant. The prediction results indicated that most of the synthesized benzopyran compounds

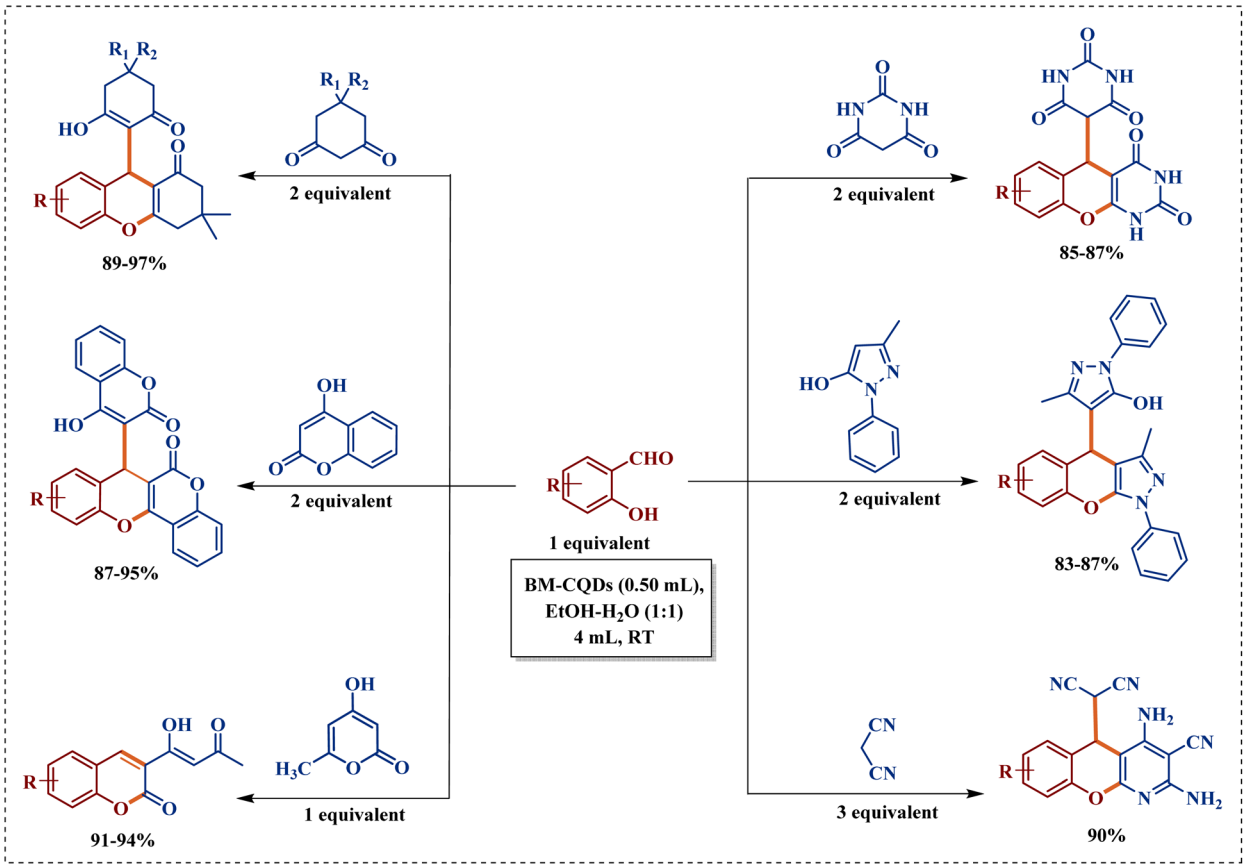

Scheme 1 General reaction schemes for synthesis of benzopyran scaffolds.

showed promising activity as neuropeptide Y5 (NPY5) receptor antagonists, testosterone 17β-dehydrogenase ($NADP^+$) inhibitors and kinase inhibitors. These three targets appeared as the most relevant among the predicted activities. The predicted biological activities along with Pa and Pi values for the representative compound **3a** are presented in Table 2.

Neuropeptide Y5 antagonists are known to play an important role in the regulation of the central nervous system. Inhibition of the NPY5 receptor is associated with neuroprotective effects and antidepressant activity, as it helps in controlling stress, anxiety, obesity, reproductive health, Alzheimer's disease, Huntington's disease, Parkinson's disease, and mood-related disorders.[55–57] Therefore, compounds showing NPY5 antagonistic behaviour may be useful for the treatment of neurological and depressive conditions. Testosterone 17β-dehydrogenase ($NADP^+$) is a key enzyme involved in steroid hormone metabolism, and its inhibition is considered important for managing hormone-related and inflammatory disorders.[46] On the other hand, the kinase inhibitors possess therapeutic potential in various areas like oncology, inflammation diseases, and neurodegenerative diseases.[58] Based on the PASS prediction results and the biological importance of these targets, they were selected for further molecular docking studies. The 3D crystal structures of the target proteins with PDB ID; 7DDZ for the NPY receptor,[59,60] 4DBW for testosterone 17β-dehydrogenase ($NADP^+$)[46] and 1A9U for kinase inhibition[61] were obtained from the RCSB Protein Data Bank,[62] and existing literature.

2.7.2. Redocking. Before docking calculations, redocking was conducted using co-crystalized ligands, H46, 511, and SB2 of the selected PDBs 7DDZ, 4DBW, and 1A9U respectively, with an aim to validate the software. As illustrated in Table 3, H46 was able to redock in enzyme 7DDZ with a docking score of -15.06 kcal mol^{-1} and RMSD value of 0.5121 Å (Fig. 12a), 511 showed docking score of -17.33 kcal mol^{-1} with a RMSD value of 0.2984 Å in 4DBW (Fig. 12b) and SB2 with docking score of -08.70 kcal mol^{-1} with RMSD of 0.7991 Å (Fig. 12c). Moreover, when comparing the interaction of the experimental co-crystalized pose with the redocked poses, it was found that all redocked poses exhibit similar interactions to the co-crystalized pose (Fig. S46). Therefore, the software was validated and docking of benzopyran derivatives was carried out.

2.7.3. Docking studies. All the seventeen benzopyran motifs were docked in the selected PDBs; 7DDZ, 4DBW and 1A9U. From molecular docking calculations, it was observed that all the synthesized benzopyran derivatives were able to dock in all the three PDBs. Also, most of the molecules showed a higher docking score than the reference (co-crystalized) in PDB IDs 7DDZ and 1A9U, however, a few in 4DBW (Table S2). From these docked candidates, common five molecules having higher docking score were selected with an aim to shortlist those compounds that possess the capability to inhibit all the

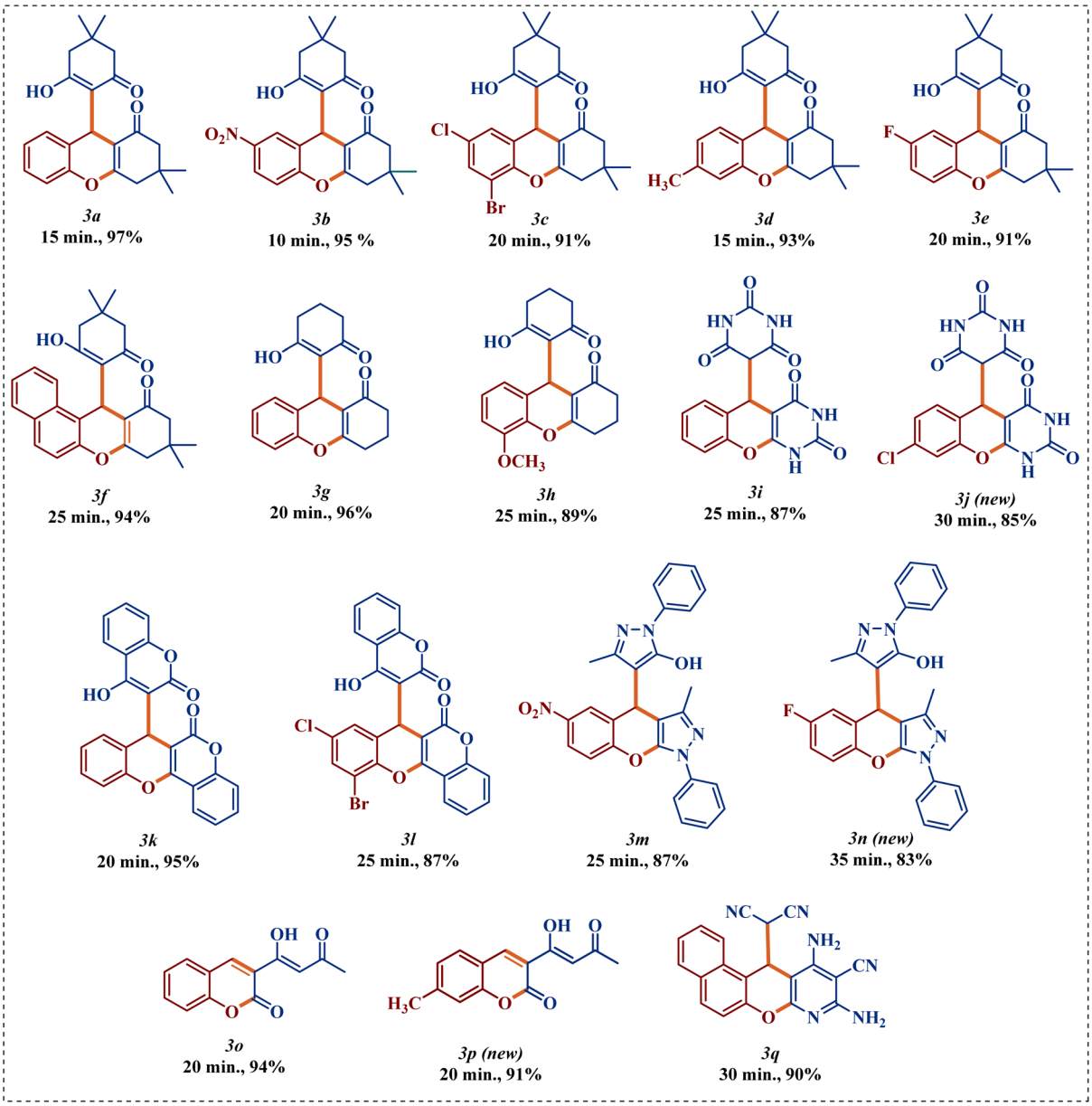

Scheme 2 Library of synthesized benzopyran compounds.

selected PDBs (Table 3). Furthermore, from 3D interaction analysis of the selected compounds interactions in the binding site of 7DDZ revealed hydrogen bonds mainly with Arg187, Cys203, and Glu205, as well as pi–pi interactions with Phe307 (Fig. 13 and 14). Thus, these molecules have the capability to act as neuropeptide Y Y2 (NYY2) receptor.[59,60] In 4DBW, common hydrogen bonds are observed with Tyr55 and His117, along with a pi–pi interaction with Trp227 (Fig. 15 and 16). As per the literature, interactions with the reported residues (Tyr55 and His177) is considered crucial for a molecule to act as the inhibitor.[63] Thus, these molecules possess the capability to act as AKR1C3 (cancer causing enzyme) inhibitor. Similarly, in 1A9U, the compound exhibited hydrogen bonds with Lys53 and Met109, and pi–pi interactions with Tyr35 (Fig. 17 and 18). The interaction with these reported resides is considered as important for a molecule to act as MEK (mitogen-activated protein kinase) inhibitor.[64,65] Thereafter, the muti-targeted screened candidates were subjected to pharmacokinetic studies using ADMET analysis.

2.7.4. ADMET analysis. The selected molecules **3i**, **3j**, **3k**, **3o**, and **3q** were subsequently evaluated for Absorption, Distribution, Metabolism, Excretion, and Toxicity (ADMET) properties using an open-access web server. The absorption parameter includes intestinal absorption (% absorbed), which represents that **3i** and **3j** may have moderate absorption while others have high absorption (Table 4). Distribution parameter includes the BBB (blood–brain barrier) permeability, which predicts that the molecules **3k**, **3o** and **3q** have good penetration (Table 4). Based

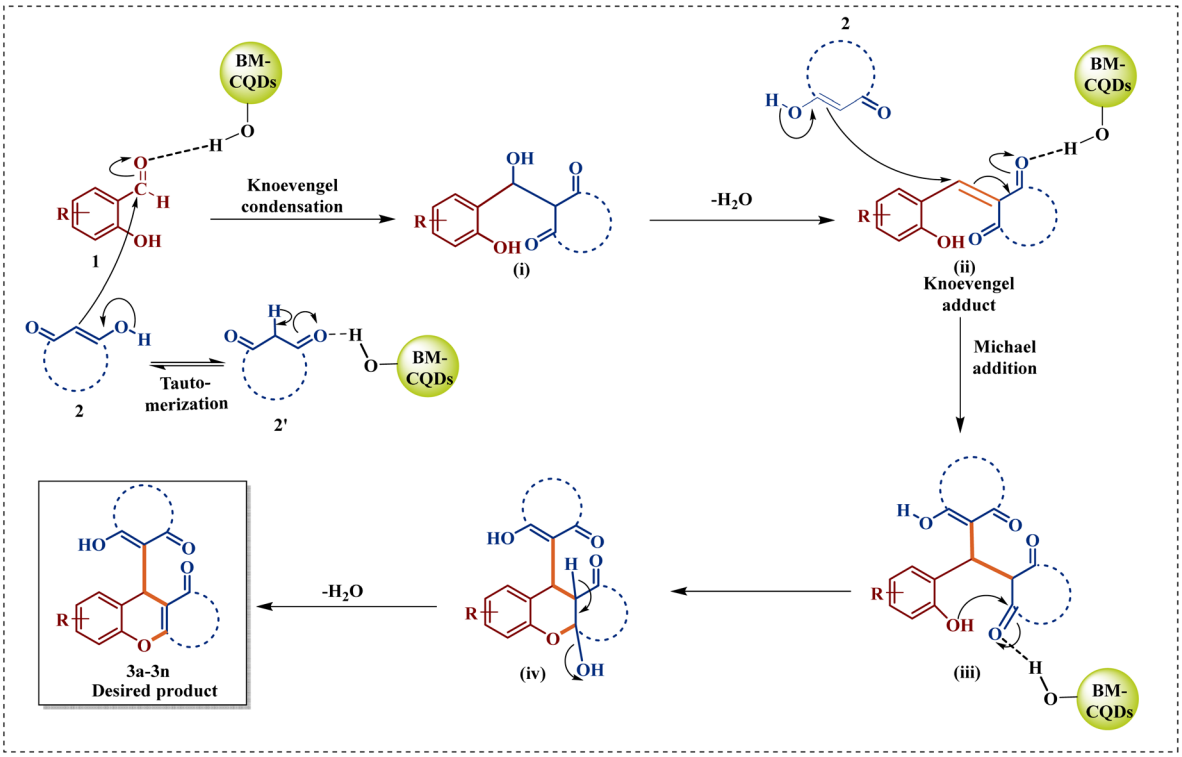

Scheme 3 Mechanistic pathway illustrating the BM-CQD-assisted formation of **3a–3n** compounds.[49]

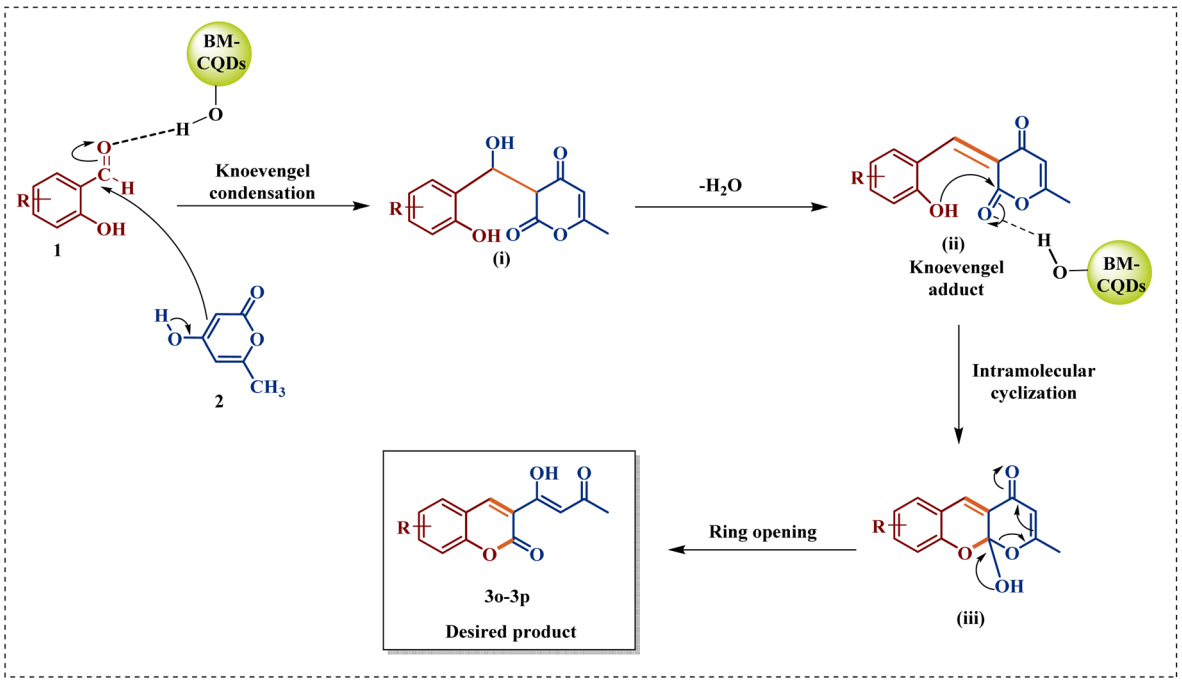

Scheme 4 Plausible mechanism for preparation of **3o–3p** scaffolds.[50]

on the metabolic parameter, all molecules were predicted to perform well, as they do not inhibit CYP2D6 enzyme (Table 4). Through total clearance, it was found that all moieties had good clearance (Table 4). Lastly, the toxic parameter was evaluated by predicting hepatotoxicity, which involves liver damage; from this, **3j** and **3o** show non-toxic behavior (Table 4).[66] Therefore, compounds **3j** and **3o** could be potential candidate that inhibits all three enzymes and can act as multi-targeted inhibitor.

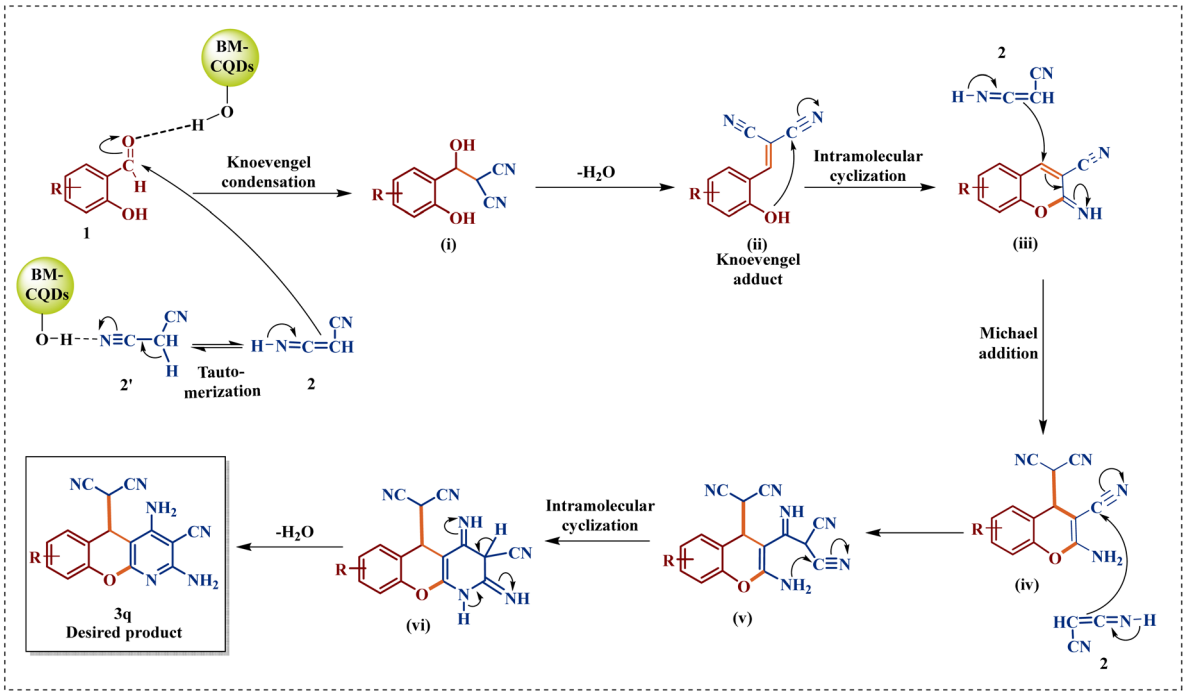

Scheme 5 Plausible pathway for the preparation of **3q** derivative.[22,51]

3. Experimental

3.1. Synthesis of BM-CQD

For the synthesis of BM-CQDs, the bark of *Butea monosperma* was collected from a small town, Bhupalsagar, Chittorgarh, Rajasthan, India (312204). The collected bark was thoroughly washed several times with water to remove dust and impurities, followed by drying under ambient conditions. The dried bark was then finely grounded to obtain a brown coloured powder. Subsequently, 4.0 g of the dried bark powder was dispersed in 80 mL of DI water and stirred magnetically for 1 h to obtain a homogeneous suspension. The resulting mixture was transferred into a Teflon-lined stainless-steel autoclave, and heated in a hot air oven at 180 °C for 18 h under hydrothermal conditions. After that, the autoclave was allowed to cool naturally to RT. A yellow-brown coloured solution (63 mL) was obtained. The solution was then centrifuged to remove larger carbonaceous residues, followed by filtration using a 0.45 μm membrane filter.

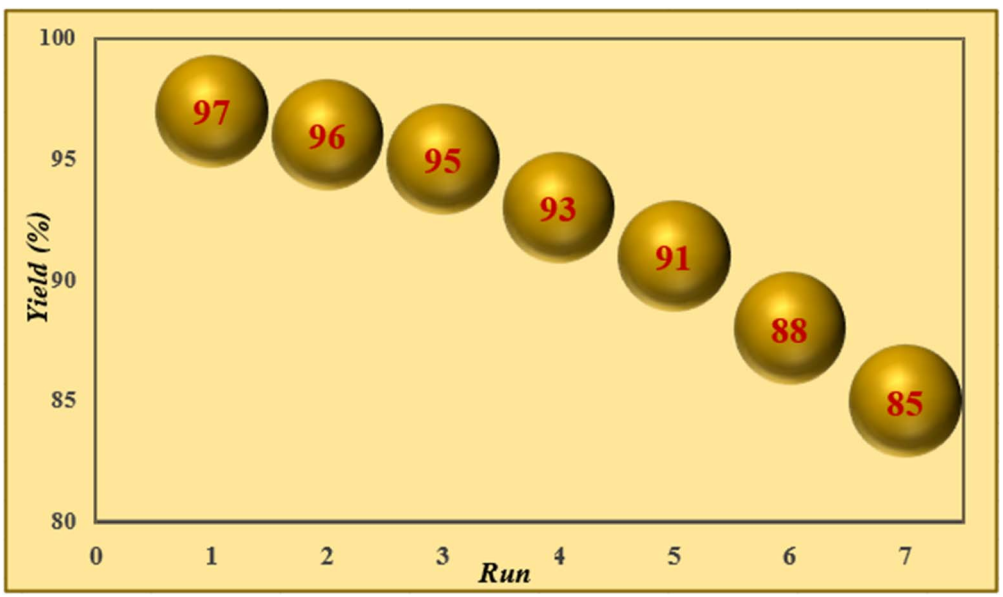

Fig. 8 Catalytic performance of BM-CQDs over seven cycles.

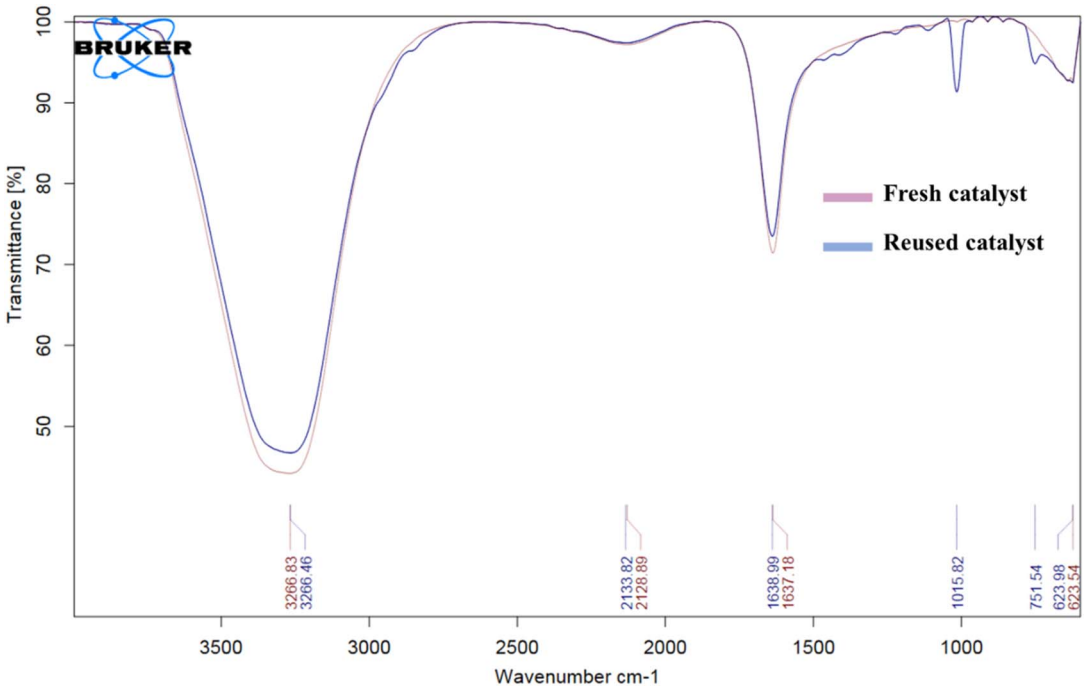

Fig. 9 Catalytic performance of BM-CQD after 7th run for the synthesis of compound **3a**.

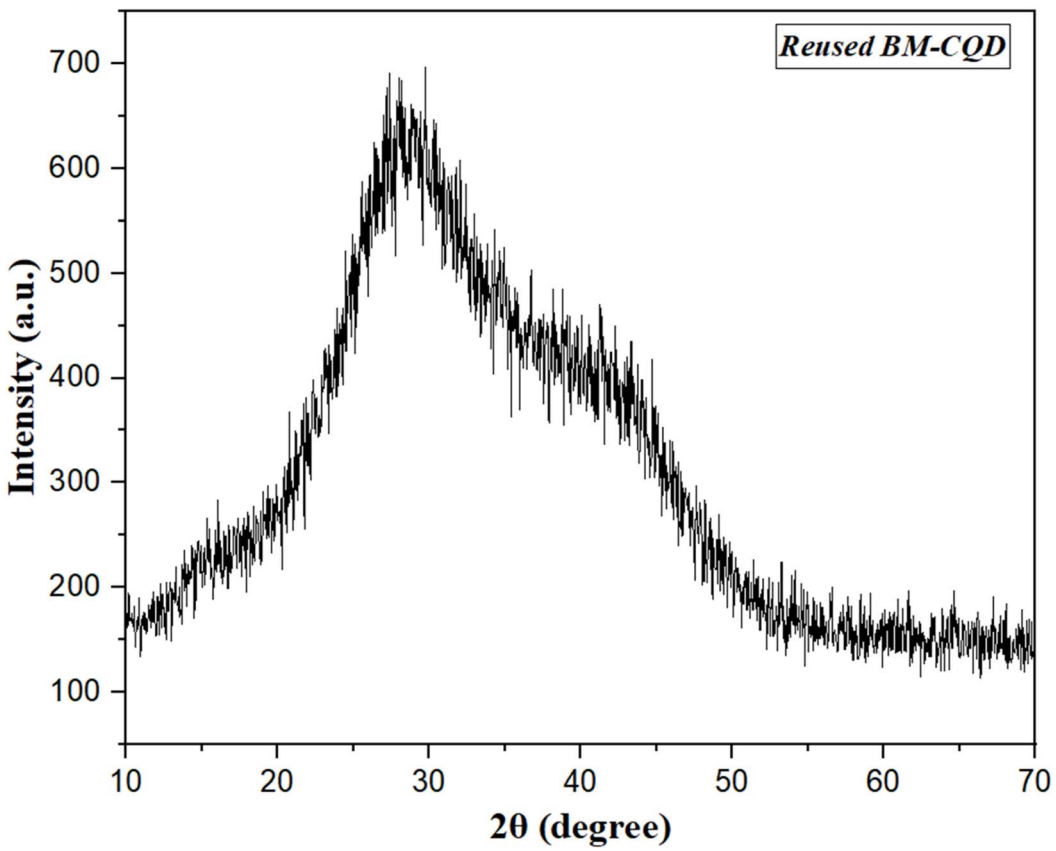

Fig. 10 XRD pattern of BM-CQD catalyst after seven cycles.

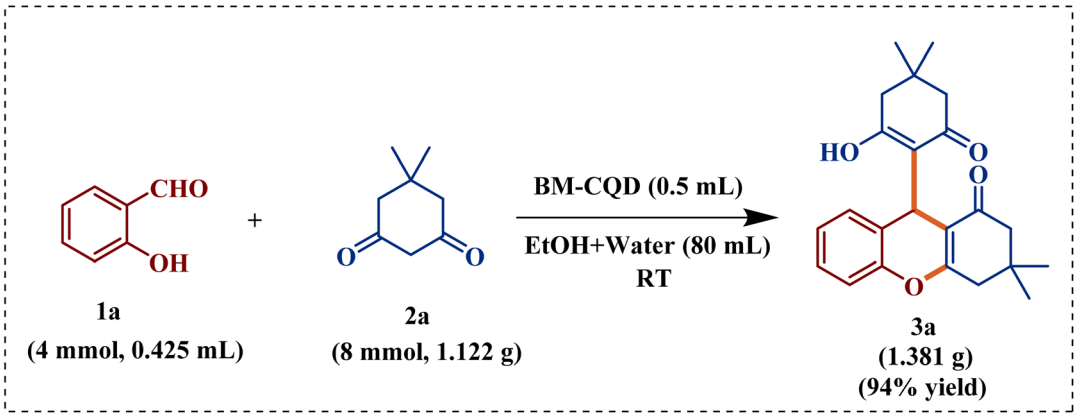

Scheme 6 Gram scale synthesis of compound **3a**.

After filtration, a clear yellow-brown BM-CQD solution (62 mL) was obtained and stored in a sealed glass vial under refrigerated conditions for further use. The synthesized BM-CQDs were obtained as a stable aqueous dispersion and used directly as a catalyst without any external support material. The complete step-wise synthesis of BM-CQDs is illustrated in Fig. 19.

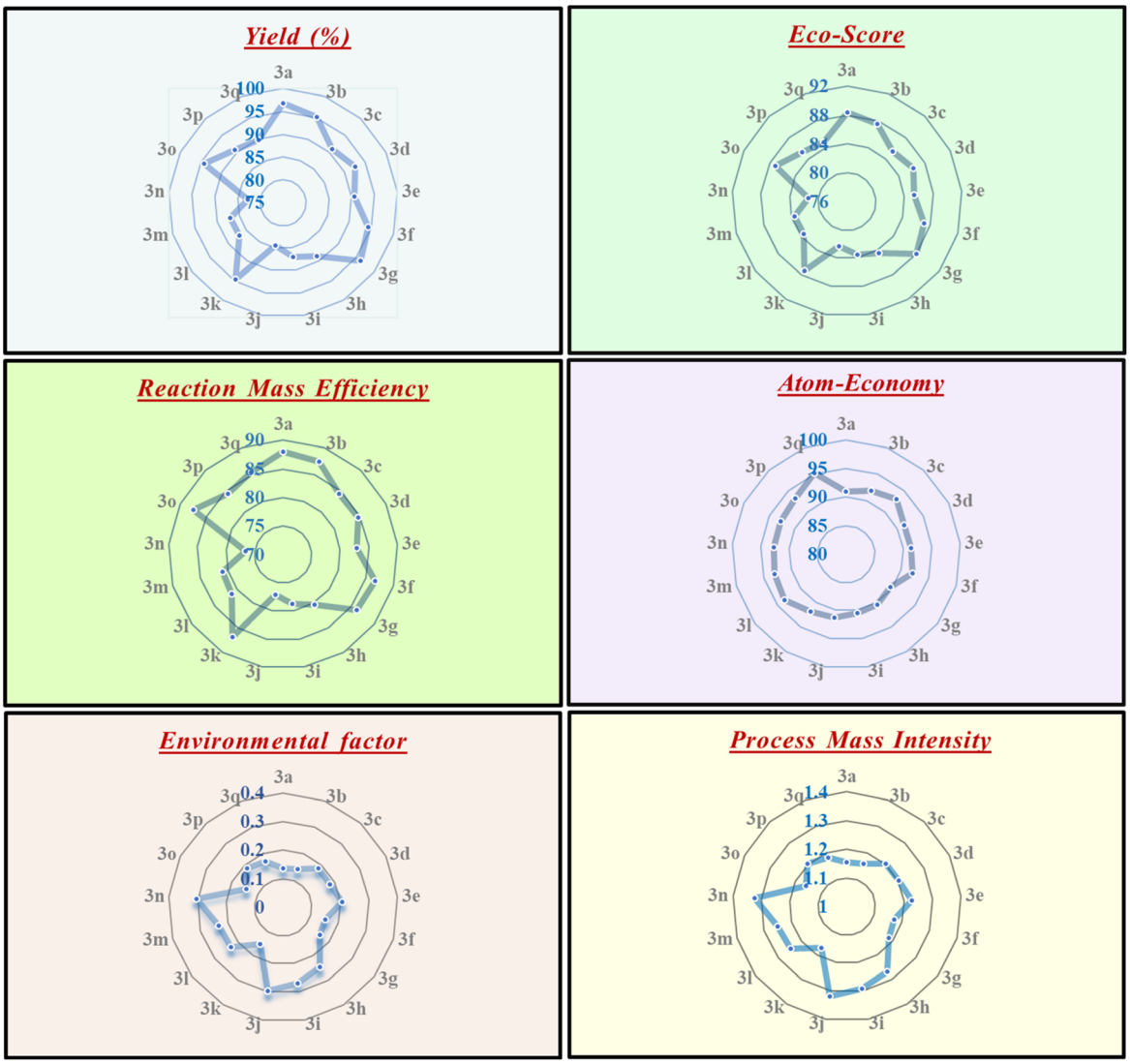

Fig. 11 Graphic representation of GCM data for all the synthesized compounds.

Table 2 The biological activities of compound '3a' were predicted using the PASS online

Pa	Pi	Activity
0,838	0,002	Neuropeptide Y5 antagonist
0,710	0,012	Kinase inhibitor
0,718	0,049	Testosterone 17beta-dehydrogenase ($NADP^+$) inhibitor
0,709	0,047	CYP2J substrate
0,618	0,012	CYP2A4 substrate
0,615	0,029	JAK2 expression inhibitor

Table 3 List of the docking score of the commonly docked candidates within the selected PDBs 7DDZ, 4DBW and 1A9U

Molecules	7DDZ (kcal mol^{-1})	Molecules	4DBW (kcal mol^{-1})	Molecules	1A9U (kcal mol^{-1})
3j	−18.91	**3q**	−19.49	**3i**	−14.35
3i	−16.34	**3k**	−19.38	**3j**	−12.49
3q	−16.33	**3j**	−18.67	**3k**	−09.44
3o	−16.30	**3o**	−17.94	**3o**	−09.20
3k	−15.99	**3i**	−17.35	**3q**	−08.89
H46	**−15.06**	**511**	**−17.33**	**SB2**	**−08.70**

The yield and concentration of the synthesized BM-CQDs were calculated using a previously reported method.[67,68] The entire BM-CQD solution was transferred into a pre-weighed beaker, and the solvent was completely evaporated by drying the sample in an oven at 80 °C. The mass of dried BM-CQDs was calculated by the difference between the final and initial weights of the beaker. The mass of dried BM-CQDs obtained was 0.982 g, while the initial biomass used was 4.0 g. The yield and concentration were calculated using the following equations:

$$\text{Yield}(\%) = \frac{\text{mass of dried BM-CQDs (g)}}{\text{mass of biomass used (g)}} \times 100$$

$$\text{Concentration}\left(\text{mg mL}^{-1}\right) = \frac{\text{mass of dried BM-CQDs (g)}}{\text{volume of BM-CQD solution(mL)}}$$

Based on these calculations, the yield of BM-CQDs was found to 24.55%, and the concentration was calculated as 15.84 mg mL^{-1}. Detailed calculations are provided in the SI.

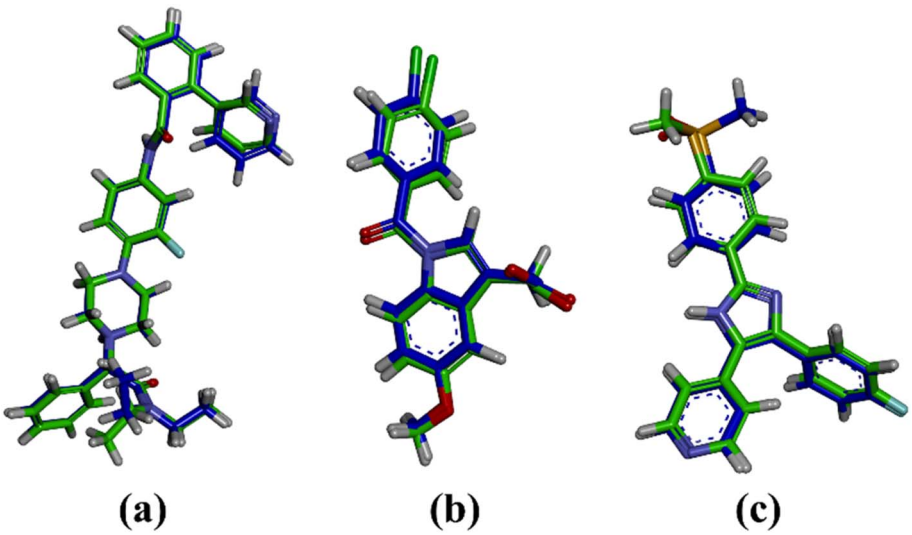

Fig. 12 Superimposed co-crystalized pose (blue) and the redocked pose (green) of (a) H46 (7DDZ), (b) 511 (4DBW) and (c) SB2 (1A9U).

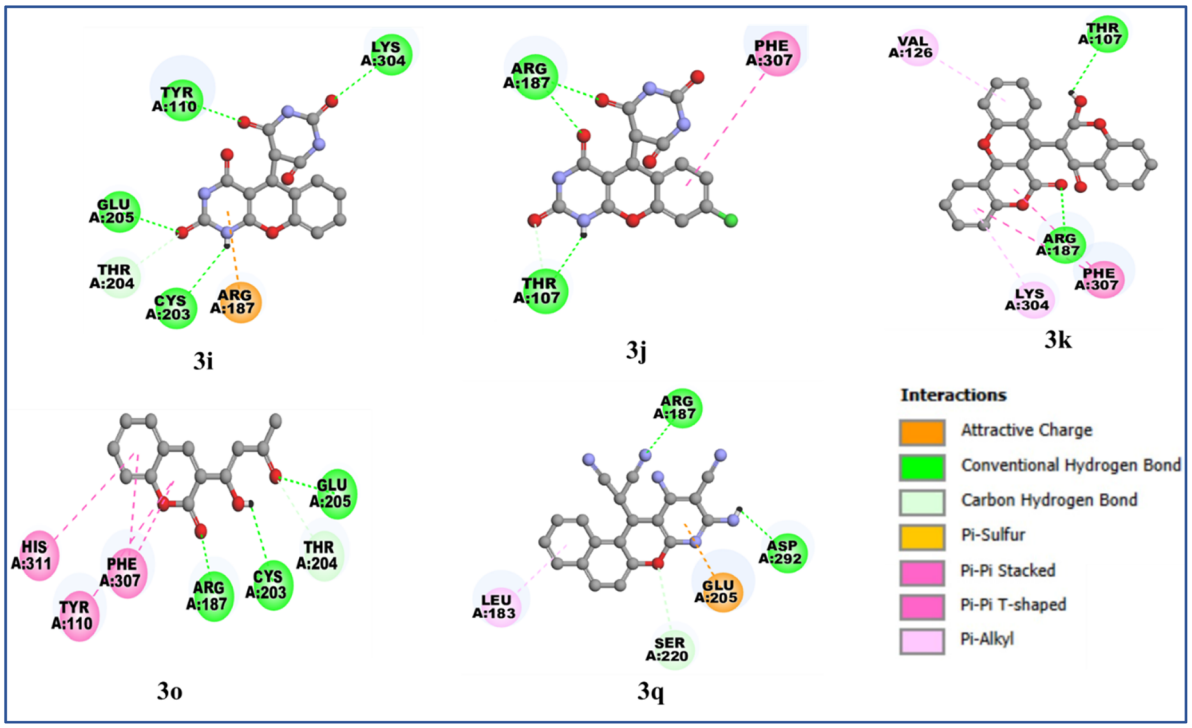

Fig. 13 2D interaction plot of the commonly selected compounds that form interaction within the binding pocket of 7DDZ.

3.2. General synthesis of benzopyran derivatives

A mixture of the appropriate salicylaldehyde derivative (1.0 equivalent, 0.5 mmol) and the corresponding C–H activated compound (1.0 equivalent, 0.5 mmol/2.0 equivalents, 1.0 mmol/3.0 equivalents, 1.5 mmol, as required) was taken in a reaction vessel containing BM-CQDs (0.5 mL) as the catalyst and an ethanol–water solvent system (4 mL). The reaction mixture was stirred at room temperature for the appropriate time. The reaction progress was monitored by TLC using hexane/ethyl acetate (7 : 3) as the eluent. Upon reaction completion, the desired benzopyran product precipitated out of the reaction mixture and isolated by simple filtration, washed thoroughly with water and then dried to afford the pure product. The

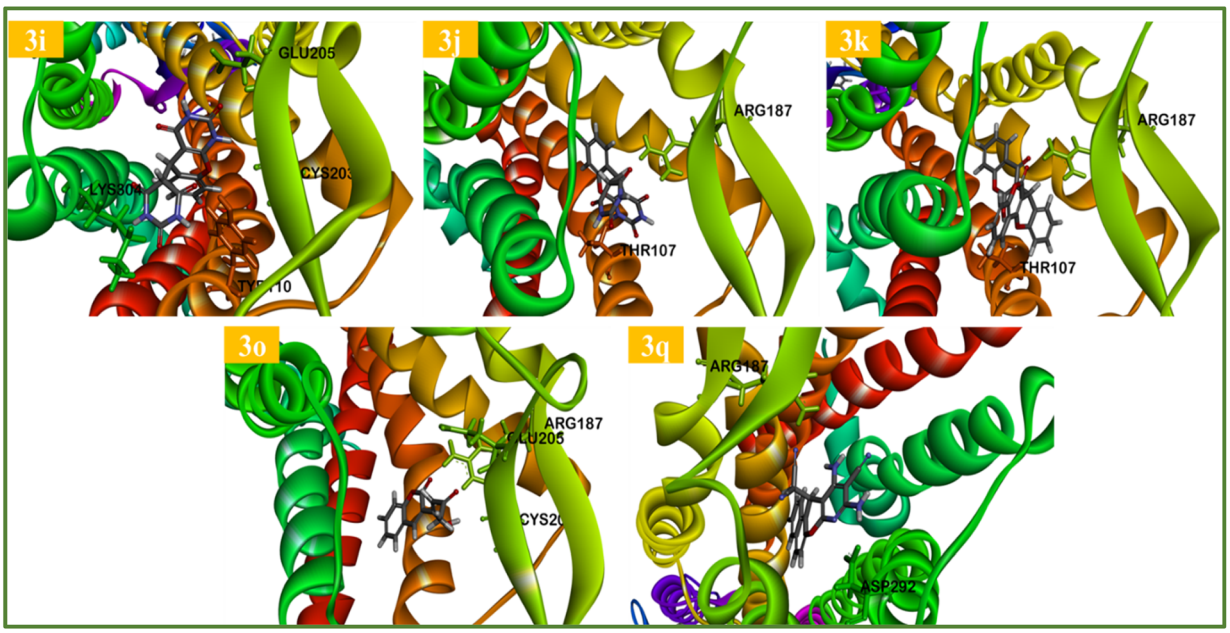

Fig. 14 3D interaction profiles of the promising compounds within the binding pocket of 7DDZ.

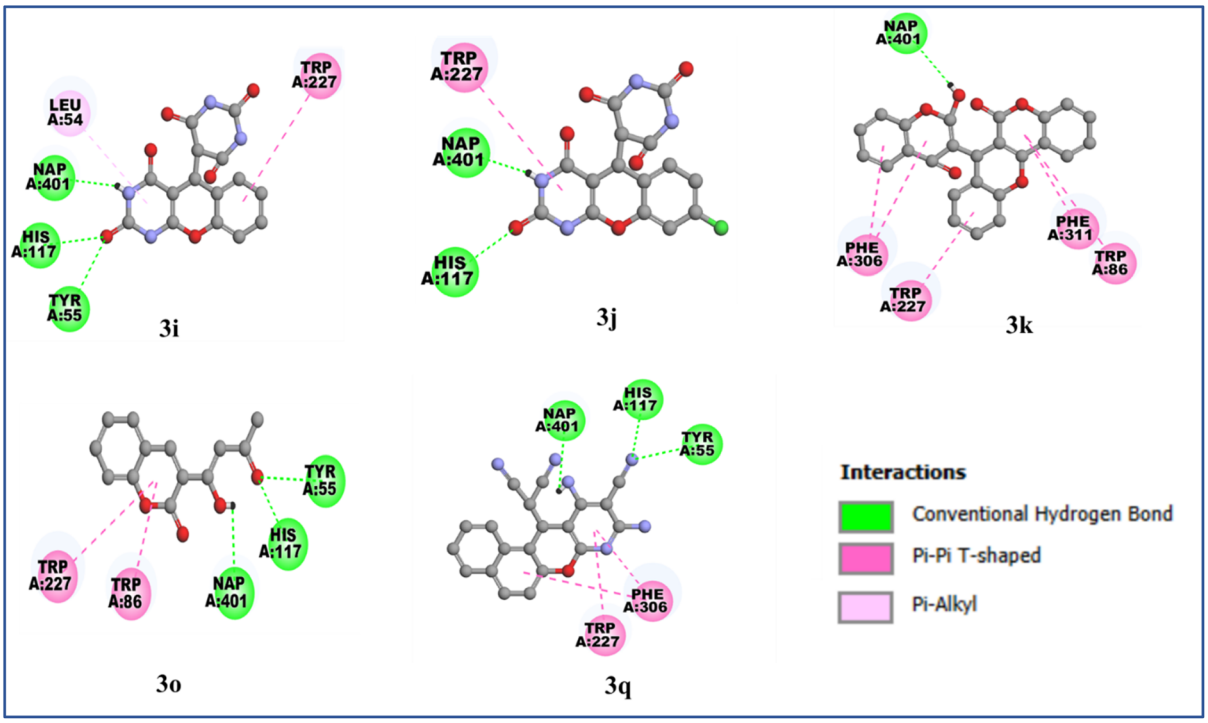

Fig. 15 2D interaction plot of the commonly selected compounds that form interaction within the binding pocket of 4DBW.

collected filtrate, containing the BM-CQD catalyst, was directly reused in subsequent reaction cycles without any further treatment, demonstrating the excellent recyclability of the catalyst.

3.3. Molecular docking studies

All the selected PDB IDs 7DDZ, 4DBW and 1A9U were imported from the RCSB database.[69] These were prepared by adding missing side chains, adding polar hydrogens, and removing crystallographic water through protein editor mode of SeeSAR.[70] Further binding site was confirmed by extracting the co-

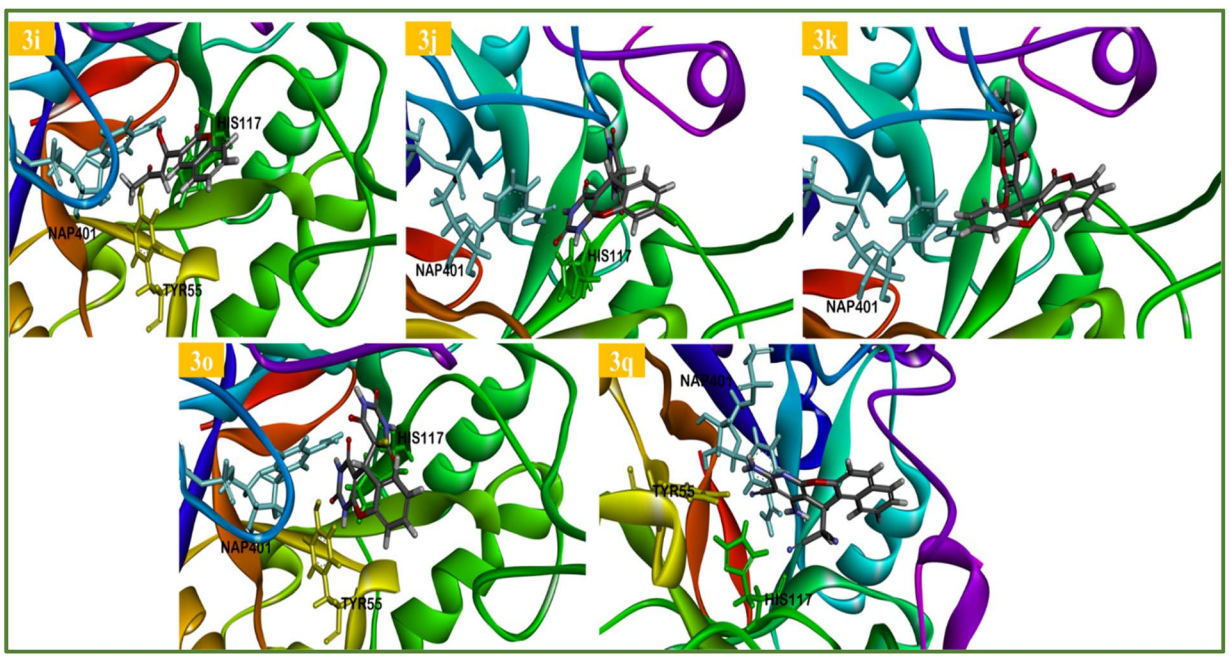

Fig. 16 3D interaction figures of the selected derivatives in the binding site of 4DBW.

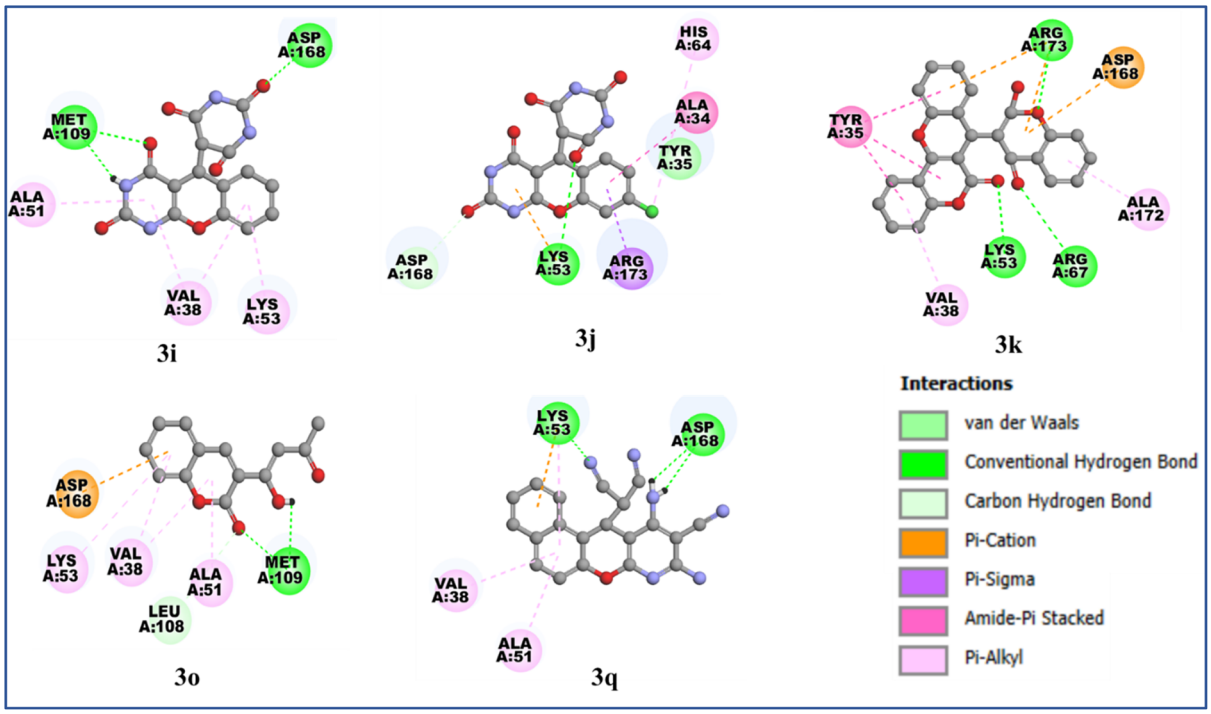

Fig. 17 2D interaction plot of the commonly selected compounds that form interaction within the binding pocket of 1A9U.

crystalized ligand bound in each PDB through the binding site mode. Molecular docking was performed using FlexX module[71] of docking mode in SeeSAR.[70] This module evaluates the docking score through an incremental construction-based algorithm, which splits the ligand into small fragments and allows them to rearrange and assemble within the selected binding pocket. During docking maximum ten poses were generated for each molecule, from which the top-scoring candidates were selected to conduct ADMET studies.

3.4. ADMET studies

The screened candidates from docking studies were converted into Simplified Molecular-Input Line-Entry System (SMILES) using Open Babel GUI.[72] Furthermore, the SMILES code of each

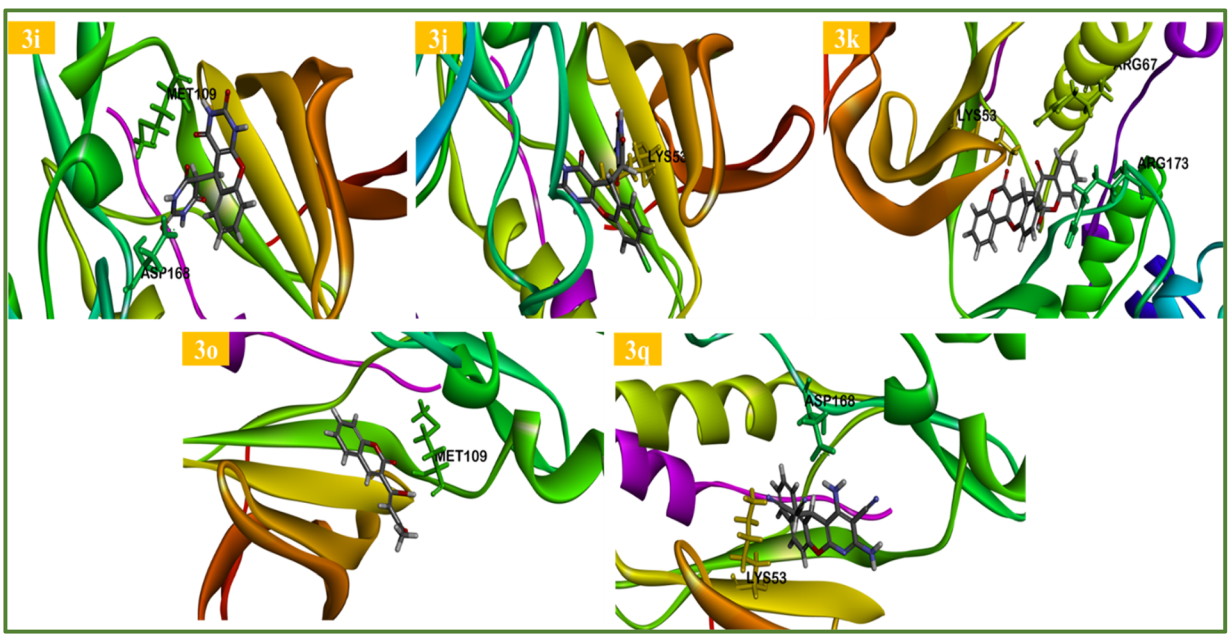

Fig. 18 3D interaction diagrams depicting the molecular interactions of selected ligands within the binding cavity of 1A9U.

Table 4 List of the ADMET properties of the commonly selected six molecules[a]

	Absorption	Distribution	Metabolism	Excretion	Toxicity
Molecules	Intestinal absorption	BBB permeability	CYP2D6 inhibitor	Total clearance	Hepatotoxicity
3i	67.146	−1.015	No	−0.02	Yes
3j	68.261	−1.188	No	−0.408	No
3k	99.007	−0.16	No	0.817	Yes
3o	94.337	−0.083	No	0.709	No
3q	96.182	−0.565	No	0.187	Yes

[a] Intestinal absorption (% absorbed): >80 (high), 50 to 80 (moderate); BBB permeability (log BB): >−1 (good); CYP2D6 inhibitor: no; total clearance: −0.3 to 0.6 (good).

compound was entered in pkCSM, an open-access web tool.[73] This tool evaluates ADMET properties like blood–brain barrier (BBB) permeability, intestinal absorption, CYP2D6 inhibitor, total clearance and hepatotoxicity. Molecules that met the acceptable range of these parameters were selected as potential candidates.

3.5. Spectral data of synthesized compounds

3.5.1. 9-(2-Hydroxy-4,4-dimethyl-6-oxocyclohex-1-en-1-yl)-3,3-dimethyl-2,3,4,9-tetrahydro-1*H*-xanthen-1-one (3a). Off white solid; yield 97%, m.p. 196–198 °C,[49,74] ^{1}H NMR (400 MHz, $CDCl_3$); δ 10.49 (s, 1H, OH), 7.16–7.12 (m, 1H, Ar–H), 7.02–6.98 (m, 3H, Ar–H), 4.65 (s, 1H, CH), 2.61–2.44 (m, 2H, CH_2), 2.36–2.31 (m, 4H, CH_2), 2.00–1.89 (m, 2H, CH_2), 1.11 (s, 3H, CH_3), 1.01 (s, 3H, CH_3), 0.97 (s, 6H, CH_3). ^{13}C NMR (101 MHz, $CDCl_3$); δ 201.08, 196.73, 170.82, 169.30, 151.10, 128.07, 127.63, 124.68, 124.38, 118.40, 115.82, 111.11, 50.65, 49.98, 43.23, 41.60, 32.41, 31.03, 30.01, 29.25, 27.84, 27.31, 26.51. ESI-MS (m/z) for $C_{23}H_{26}O_4$; 366.1831 [M^+].

3.5.2. 9-(2-Hydroxy-4,4-dimethyl-6-oxocyclohex-1-en-1-yl)-3,3-dimethyl-7-nitro-2,3,4,9-tetrahydro-1*H*-xanthen-1-one (3b). White powder, yield 95%, m.p. 192–195 °C,[75] ^{1}H NMR (400 MHz, $CDCl_3$); δ 10.33 (s, 1H, OH), 8.03 (dd, J = 8.9, 2.7 Hz, 1H, Ar–H), 7.92 (d, J = 2.5 Hz, 1H, Ar–H), 7.10 (d, J = 8.9 Hz, 1H, Ar–H), 4.67 (s, 1H, CH), 2.62–2.33 (m, 6H, CH_2), 1.96 (q, J = 16.6 Hz, 2H, CH_2), 1.13 (s, 3H, CH_3), 0.99 (d, J = 14.8 Hz, 9H, CH_3). ^{13}C NMR (101 MHz, $CDCl_3$); δ 200.98, 196.98, 172.09, 167.99, 155.49, 144.32, 126.00, 123.84, 123.69, 117.71, 116.51, 110.99, 50.59, 49.95, 43.22, 41.25, 32.44, 31.25, 29.73, 29.27, 27.93, 27.13, 26.74. ESI-MS (m/z) calculated for $C_{23}H_{25}NO_6$ [M + 1]: 412.1682 and found 412.1763.

3.5.3. 5-Bromo-7-chloro-9-(2-hydroxy-4,4-dimethyl-6-oxocyclohex-1-en-1-yl)-3,3-dimethyl-2,3,4,9-tetrahydro-1*H*-xanthen-1-one (3c). Fluffy white, yield 91%, m.p. 236–238 °C,[31] ^{1}H NMR (400 MHz, DMSO-d_6); δ 10.76 (s, 1H, OH), 7.51 (d, J = 2.5 Hz, 1H, Ar–H), 6.84 (d, J = 2.1 Hz, 1H, Ar–H), 5.01 (s, 1H, CH), 2.57–2.50

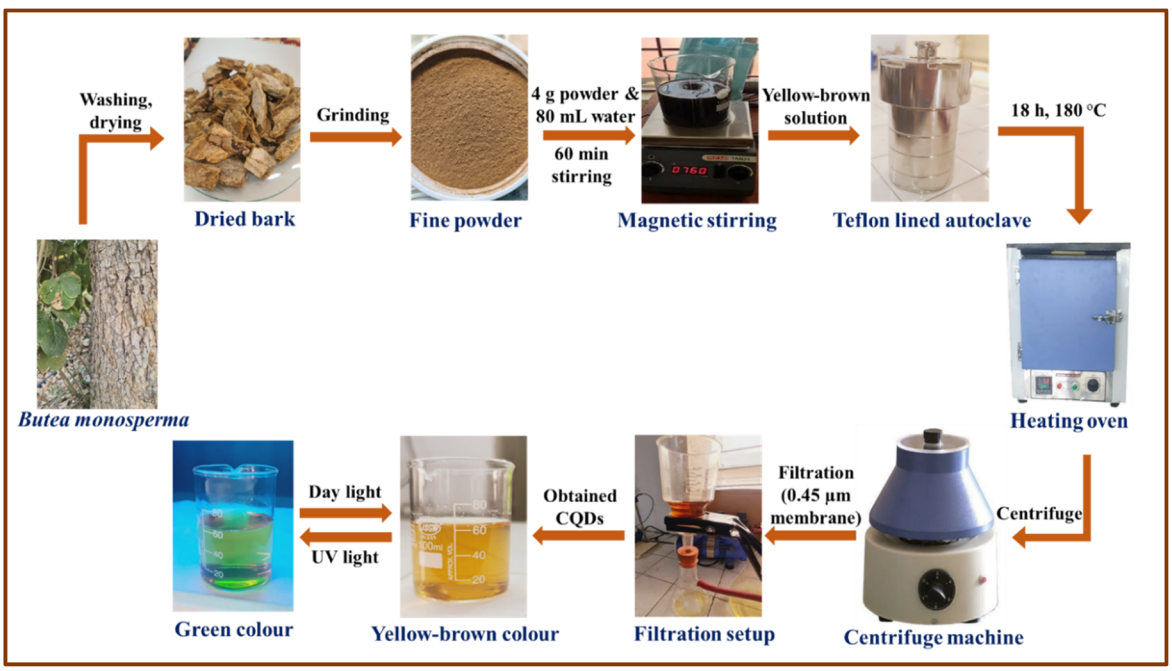

Fig. 19 Step-wise hydrothermal synthesis of BM-CQDs.

(m, 1H, CH_2), 2.35–1.98 (m, 7H, CH_2), 1.01 (s, 3H, CH_3), 0.92 (s, 3H, CH_3), 0.84 (s, 6H, CH_3). ^{13}C NMR (101 MHz, DMSO-d_6); δ 197.61, 196.19, 164.85, 164.68, 146.14, 130.25, 129.69, 128.37, 127.66, 120.59, 111.21, 110.49, 50.82, 50.35, 43.28, 40.79, 32.24, 32.15, 29.64, 29.04, 28.12, 27.05, 26.49. ESI-MS (m/z) for $C_{23}H_{24}BrClO_4$: 478.0546 [M^+].

3.5.4. 9-(2-Hydroxy-4,4-dimethyl-6-oxocyclohex-1-en-1-yl)-3,3,6-trimethyl-2,3,4,9-tetrahydro-1*H*-xanthen-1-one (3d). Off white powder, yield 93%, m.p. 202–204 °C,[28] ^{1}H NMR (400 MHz, $CDCl_3$); δ 10.48 (s, 1H, OH), 6.87–6.80 (m, 3H, Ar–H), 4.62 (s, 1H, CH), 2.55–2.31 (m, 6H, CH_2), 2.28 (s, 3H, CH_3), 1.95 (q, J = 16.5 Hz, 2H, CH_2), 1.10 (s, 3H, CH_3), 0.99 (d, J = 14.1 Hz, 9H, CH_3). ^{13}C NMR (101 MHz, $CDCl_3$); δ 201.03, 196.79, 170.73, 169.34, 150.86, 137.60, 127.76, 125.58, 121.26, 118.43, 116.34, 111.22, 50.71, 50.00, 43.23, 41.64, 32.41, 31.03, 30.01, 29.20, 27.54, 27.38, 26.52, 21.23. ESI-MS (m/z) for $C_{24}H_{28}O_4$: 380.1988 [M^+].

3.5.5. 7-Fluoro-9-(2-hydroxy-4,4-dimethyl-6-oxocyclohex-1-en-1-yl)-3,3-dimethyl-2,3,4,9-tetrahydro-1*H*-xanthen-1-one (3e). White solid, yield 91%, m.p. 198–201 °C,[28] ^{1}H NMR (400 MHz, $CDCl_3$); δ 10.48 (s, 1H, OH), 6.98–6.95 (m, 1H, Ar–H), 6.85–6.80 (m, 1H, Ar–H), 6.69 (dd, J = 8.6, 2.9 Hz, 1H, Ar–H), 4.62 (s, 1H, CH), 2.59–2.31 (m, 6H, CH_2), 2.01–1.92 (m, 2H, CH_2), 1.11 (s, 3H, CH_3), 1.00–0.98 (m, 9H, CH_3). ^{13}C NMR (101 MHz, $CDCl_3$); δ 200.98, 196.79, 171.34, 169.17, 159.43 (d, J = 242.7 Hz, C–F), 147.23 (d, J = 2.9 Hz), 126.19 (d, J = 7.9 Hz), 117.89, 116.94 (d, J = 8.9 Hz), 114.39 (d, J = 7.5 Hz), 114.15 (d, J = 7.5 Hz), 110.27, 50.67, 49.97, 43.26, 41.54, 32.37, 31.08, 29.90, 29.29, 28.21, 27.19, 26.65. ^{19}F NMR (376 MHz, $CDCl_3$); δ −118.33 (s). ESI-MS (m/z) for $C_{23}H_{25}FO_4$: 384.1737 [M^+].

3.5.6. 12-(2-Hydroxy-4,4-dimethyl-6-oxocyclohex-1-en-1-yl)-9,9-dimethyl-8,9,10,12-tetrahydro-11*H*-benzo[*a*]xanthen-11-one (3f). White powder, yield 94%, m.p. 238–240 °C,[75] ^{1}H NMR (400 MHz, $CDCl_3$); δ 10.68 (s, 1H, OH), 7.76–7.68 (m, 3H, Ar–H), 7.46–7.23 (m, 3H, Ar–H), 5.24 (s, 1H, CH), 2.67–2.52 (m, 2H, CH_2), 2.43–2.33 (m, 4H, CH_2), 1.96–1.71 (m, 2H, CH_2), 1.14 (s, 3H, CH_3), 1.04 (s, 3H, CH_3), 0.92 (s, 3H, CH_3), 0.69 (s, 3H, CH_3). ^{13}C NMR (101 MHz, $CDCl_3$); δ 201.17, 196.96, 170.34, 169.16, 148.96, 131.34, 131.05, 128.63, 128.57, 126.79, 124.73, 122.96, 117.75, 116.67, 116.22, 111.15, 50.78, 50.05, 43.27, 41.44, 32.49, 30.72, 30.00, 29.44, 27.15, 26.47, 25.46. ESI-MS (m/z) for $C_{27}H_{28}O_4$: 416.1988 [M^+].

3.5.7. 9-(2-Hydroxy-6-oxocyclohex-1-en-1-yl)-2,3,4,9-tetrahydro-1*H*-xanthen-1-one (3g). White solid, yield 96%, m.p. 220–222 °C,[28] ^{1}H NMR (400 MHz, $CDCl_3$); δ 10.84 (s, 1H, OH), 7.17–7.12 (m, 1H, Ar–H), 7.02–6.99 (m, 3H, Ar–H), 4.62 (s, 1H, CH), 2.78–2.71 (m, 1H, CH_2), 2.62–2.49 (m, 3H, CH_2), 2.45–2.35 (m, 2H, CH_2), 2.16–1.70 (m, 6H, CH_2). ^{13}C NMR (101 MHz, $CDCl_3$); δ 201.65, 197.24, 172.99, 171.30, 150.94, 128.15, 127.62, 124.74, 127.68, 119.92, 115.62, 112.37, 37.06, 36.09, 29.81, 28.09, 28.08, 19.98, 19.70. ESI-MS (m/z) for $C_{19}H_{18}O_4$: 310.1205 [M^+].

3.5.8. 9-(2-Hydroxy-6-oxocyclohex-1-en-1-yl)-5-methoxy-2,3,4,9-tetrahydro-1*H*-xanthen-1-one (3h). Fluffy white solid, yield 89%, m.p. 232–235 °C,[75] ^{1}H NMR (400 MHz, DMSO-d_6); δ 10.45 (s, 1H, OH), 6.88–6.84 (m, 1H, Ar–H), 6.78–6.71 (m, 1H, Ar–H), 6.52–6.50 (m, 1H, Ar–H), 5.02 (s, 1H, CH), 3.73 (s, 3H, OCH_3), 2.52–2.48 (m, 1H, CH_2), 2.22–2.16 (m, 6H, CH_2), 1.90–1.63 (m, 5H, CH_2). ^{13}C NMR (101 MHz, DMSO-d_6); δ 204.71, 196.58, 167.01, 147.13, 139.54, 126.85, 124.39, 120.21, 112.27, 110.05, 101.50, 101.09, 55.97 (OCH_3), 37.18, 36.33, 27.81, 25.82, 24.01, 23.95, 20.83. ESI-MS (m/z) for $C_{20}H_{20}O_5$: 340.1311 [M^+].

3.5.9. 5-(2,4-Dioxo-1,3,4,5-tetrahydro-2*H*-chromeno[2,3-*d*]pyrimidin-5-yl)pyrimidine-2,4,6(1*H*,3*H*,5*H*)-trione (3i). Off white powder, yield 87%, m.p. 218–220 °C,[49,74] ^{1}H NMR (400 MHz, DMSO-d_6); δ 11.96 (s, 1H, NH), 11.28 (s, 1H, NH), 11.16 (s, 1H, NH), 10.97 (s, 1H, NH), 7.32–7.28 (m, 1H, Ar–H), 7.19–7.15 (m, 1H, Ar–H), 7.10–7.04 (m, 2H, Ar–H), 4.67 (d, J = 2.3 Hz, 1H, CH), 3.80 (d, J = 2.4 Hz, 1H, CH). ^{13}C NMR (101 MHz, DMSO-d_6); δ 170.17, 169.50, 164.04, 155.91, 151.10, 150.08, 149.61, 131.14, 129.77, 128.56, 126.13, 117.01, 85.71, 54.40, 34.12. ESI-MS (m/z) for $C_{15}H_{10}N_4O_6$: 342.0600 [M^+].

3.5.10. 5-(8-Chloro-2,4-dioxo-1,3,4,5-tetrahydro-2*H*-chromeno[2,3-*d*]pyrimidin-5-yl)pyrimidine-2,4,6(1*H*,3*H*,5*H*)-trione (3j). Off white solid, yield 85%, m.p. 290–292 °C[new], ^{1}H NMR (400 MHz, DMSO-d_6); δ 12.07 (s, 1H, NH), 11.31 (s, 1H, NH), 11.21 (s, 1H, NH), 11.04 (s, 1H, NH), 7.29–7.03 (m, 3H, Ar–H), 4.67 (d, J = 1.6 Hz, 1H, CH), 3.85 (d, J = 2.1 Hz, 1H, CH). ^{13}C NMR (101 MHz, DMSO-d_6); δ 169.96, 169.37, 163.94, 155.59, 151.08, 150.20 149.99, 133.44, 130.14, 126.23, 120.92, 116.96, 85.72, 53.92, 33.34. ESI-MS (m/z) calculated for $C_{15}H_9ClN_4O_6$: 377.0211 [M + 1] and found 377.0289.

3.5.11. 7-(4-Hydroxy-2-oxo-2*H*-chromen-3-yl)-6*H*,7*H*-chromeno[4,3-*b*]chromen-6-one (3k). White powder, yield 95%, m.p. 237–239 °C,[76] ^{1}H NMR (400 MHz, $CDCl_3$); δ 10.41 (s, 1H, OH), 8.14 (dd, J = 8.0, 1.6 Hz, 1H, Ar–H), 8.02 (dd, J = 8.0, 1.6 Hz, 1H, Ar–H), 7.64–7.60 (m, 1H, Ar–H), 7.50–7.39 (m, 3H, Ar–H), 7.33–7.27 (m, 3H, Ar–H), 7.19–7.17 (m, 1H, Ar–H), 7.13–7.08 (m, 2H, Ar–H), 5.36 (s, 1H, CH). ^{13}C NMR (101 MHz, $CDCl_3$); δ 166.26, 161.53, 161.33, 158.89, 153.11, 152.14, 151.01, 132.90, 132.07, 128.84, 128.64, 125.66, 125.13, 124.44, 123.98, 123.50, 121.44, 117.07, 116.89, 116.42, 116.36, 114.65, 108.71, 100.24, 30.01. ESI-MS (m/z) for $C_{25}H_{14}O_6$: 410.0790 [M^+].

3.5.12. 11-Bromo-9-chloro-7-(4-hydroxy-2-oxo-2*H*-chromen-3-yl)-6*H*,7*H*-chromeno[4,3-*b*]chromen-6-one (3l). Off white, yield 87%, m.p. 203–205 °C,[77] ^{1}H NMR (400 MHz, DMSO-d_6); δ 10.80 (s, 1H, OH), 8.08–7.96 (m, 2H, Ar–H), 7.71–7.68 (m, 2H, Ar–H), 7.57 (s, 1H, Ar–H), 7.48–7.41 (m, 2H, Ar–H), 7.31 (s, 2H, Ar–H), 7.22–7.15 (m, 1H, Ar–H), 5.68 (s, 1H, CH). ^{13}C NMR (101 MHz, DMSO-d_6); δ 164.44, 161.97, 160.47, 156.08, 152.81, 152.45, 151.21, 133.41, 133.04, 131.65, 129.65, 128.09, 126.31, 125.38, 124.62, 124.53, 122.75, 120.14, 117.18, 116.88, 116.54, 113.83, 111.31, 107.36, 29.74. ESI-MS (m/z) for $C_{25}H_{12}BrClO_6$: 521.9506 [M^+].

3.5.13. 3-Methyl-4-(3-methyl-6-nitro-1-phenyl-1,4-dihydrochromeno[2,3-*c*]pyrazol-4-yl)-1-phenyl-1*H*-pyrazol-5-ol (3m). Light yellow powder, yield 87%, m.p. 228–230 °C,[78] ^{1}H NMR (400 MHz, DMSO-d_6); δ 11.33 (s, 1H, OH), 8.48 (s, 1H, Ar–H), 7.98 (d, J = 7.6 Hz, 1H, Ar–H), 7.68–7.66 (m, 4H, Ar–H), 7.41 (s, 4H, Ar–H), 7.22 (s, 2H, Ar–H), 6.92 (d, J = 8.6 Hz, 1H, Ar–H), 5.12 (s, 1H, CH), 2.28 (s, 6H, CH_3). ^{13}C NMR (101 MHz, DMSO-d_6); δ 161.38, 146.78, 139.79, 130.42, 129.51, 126.27, 125.28, 124.51, 121.24, 115.76, 28.19, 12.18. ESI-MS (m/z) calculated for $C_{27}H_{21}N_5O_4$: 479.1594 [M + 1] and found 480.1667.

3.5.14. 4-(6-Fluoro-3-methyl-1-phenyl-1,4-dihydrochromeno[2,3-*c*]pyrazol-4-yl)-3-methyl-1-phenyl-1*H*-

pyrazol-5-ol (3n). Off white powder, yield 83%, m.p. 204–206 °C[new], ^{1}H NMR (400 MHz, DMSO-d_6); δ 7.67 (d, J = 7.4 Hz, 4H, Ar–H), 7.42–7.31 (m, 5H, Ar–H), 7.22 (d, J = 6.2 Hz, 2H, Ar–H), 6.81–6.72 (m, 2H, Ar–H), 5.13 (s, 1H, CH), 2.27 (s, 6H, CH_3). ^{13}C NMR (101 MHz, DMSO-d_6); δ 155.68 (d, J = 232.9 Hz, C–F), 150.68, 146.79, 131.45, 129.47, 126.17 (d, J = 5.4 Hz), 121.28, 115.96 (d, J = 9.5 Hz), 115.60 (d, J = 23.8 Hz), 113.55 (d, J = 22.7 Hz), 113.28, 28.04, 12.27. ^{19}F NMR (376 MHz, DMSO-d_6); δ −125.30 (s). ESI-MS (m/z) calculated for $C_{27}H_{21}FN_4O_2$: 453.1649 [M + 1] and found 453.1736.

3.5.15. 3-(1-Hydroxy-3-oxobut-1-en-1-yl)-2*H*-chromen-2-one (3o). Pale yellow solid, yield 94%, m.p. 134–136 °C,[50] ^{1}H NMR (400 MHz, $CDCl_3$); δ 8.65 (s, 1H, CH), 7.65–7.61 (m, 2H, Ar–H), 7.397–7.32 (m, 2H, Ar–H), 7.02 (s, 1H, Ar–H of pyrone ring), 2.26 (s, 3H, CH_3). ^{13}C NMR (101 MHz, $CDCl_3$); δ 200.01, 171.95, 158.20, 154.47, 145.61, 134.11, 129.66, 125.08, 120.66, 118.61, 116.69, 101.74, 27.74. ESI-MS (m/z) calculated for $C_{13}H_{10}O_4$: 231.0579 [M + 1] and found 231.0659.

3.5.16. 3-(1-Hydroxy-3-oxobut-1-en-1-yl)-7-methyl-2*H*-chromen-2-one (3p). Light yellow powder, yield 91%, m.p. 137–140 °C[new], ^{1}H NMR (400 MHz, $CDCl_3$); δ 8.59 (s, 1H, CH), 7.52–7.48 (m, 1H, Ar–H), 7.14–7.12 (m, 2H, Ar–H), 6.99 (s, 1H, Ar–H of pyrone ring), 2.46 (s, 3H, CH_3), 2.24 (s, 3H, CH_3). ^{13}C NMR (101 MHz, $CDCl_3$); δ 199.54, 172.60, 158.41, 154.67, 146.08, 145.63, 129.36, 126.40, 119.37, 116.79, 116.30, 101.44, 27.57, 22.26. ESI-MS (m/z) calculated for $C_{14}H_{12}O_4$: 245.0736 [M + 1] and found 245.0824.

3.5.17. 2-(9,11-Diamino-10-cyano-12*H*-benzo[5,6]chromeno[2,3-*b*]pyridin-12 yl)malononitrile (3q). Yellow solid, yield 90%, m.p. >300 °C,[79] ^{1}H NMR (400 MHz, DMSO-d_6); δ 8.38 (d, J = 8.6 Hz, 1H, Ar–H), 7.99–7.93 (m, 2H, Ar–H), 7.64–7.38 (m, 3H, Ar–H), 7.23 (s, 2H, NH_2), 6.76 (s, 2H, NH_2), 5.92 (d, J = 4.5 Hz, 1H, C**H**-$(CN)_2$), 5.01 (d, J = 4.6 Hz, 1H, CH). ^{13}C NMR (101 MHz, DMSO-d_6); δ 161.40 (N–**C**–O), 161.01, 157.76, 151.01, 131.23, 131.08, 130.85, 129.08, 127.56, 125.75, 123.99, 118.07, 116.96, 113.86 and 113.73, 112.19, 85.05, 71.21, 31.01, 30.25; ESI-MS (m/z) for $C_{20}H_{12}N_6O$: 352.1073 [M^+].

4. Conclusion

In conclusion, a green and sustainable method has been developed for the synthesis of benzopyran derivatives using *Butea monosperma* bark-derived carbon quantum dots as a sustainable nanocatalyst (BM-CQDs). The synthesized catalyst was comprehensively analyzed using HRTEM, SAED, EDX, FT-IR, XRD, UV-visible, and fluorescence spectroscopy. FT-IR spectroscopy identified abundant surface –OH and –COOH functionalities, and XRD validated the low graphitization and amorphous carbon framework. Furthermore, UV-visible study revealed characteristic absorption features which further indicate the presence of conjugated carbon structures and oxygen-containing functional groups on the surface of the BM-CQDs. HRTEM and SAED analyses confirmed the uniform morphology, nanoscale size, and amorphous nature of BM-CQDs, while EDX showed their oxygen-rich composition. These findings confirm the successful synthesis of the BM-CQDs which exhibits superior catalytic performance for synthesis of benzopyran. The protocol carried out under mild conditions which avoids harsh reagents or specialized equipment, and gave excellent yields of benzopyrans within short reaction times (less than 35 min). The BM-CQDs demonstrated high catalytic efficiency across a wide range of substituted salicylaldehydes and C–H activated compounds. Gram-scale synthesis with excellent yield and recyclability up to seven cycles further confirmed the practical and economic viability of the protocol. Additionally, favourable green chemistry metrics data underscore the environmental advantages of the developed approach over conventional protocols. Molecular docking studies exhibit promising interactions of benzopyran derivatives with selected biologically relevant targets, suggesting their potential therapeutic relevance. Overall, this work not only introduces a value-added application of biomass-derived CQDs in organic synthesis but also provides a sustainable platform for the rapid synthesis of benzopyran scaffolds as biologically important targets.

Consent for publication

Yes, by all authors.

Author contributions

ST performed the original research, wrote the manuscript. SS helped in editing and revising. NR and AM performed the docking studies. SA contributed to guiding, writing, revising the manuscript and overall supervision.

Conflicts of interest

The authors confirmed that this article has no conflict of interest.

Abbreviations

BM-CQDs	*Butea monosperma* bark derived carbon quantum dots
NPY5	Neuropeptide Y5
HRTEM	High resolution transmission electron microscopy
SAED	Selected area electron diffraction
EDX	Energy-dispersive X-ray spectroscopy
FT-IR	Fourier-transform infrared spectroscopy
XRD	X-ray diffraction
AcOH	Acetic acid
NMR	Nuclear magnetic resonance spectroscopy
HRMS	High resolution mass spectrometry
Pa	Probability to be active
Pi	Probability to be inactive
PASS	Prediction of activity spectra for substances
RCSB	Research collaboratory for structural bioinformatics
PDB	Protein data bank
RMSD	Root mean square deviation
GCM	Green chemistry metrics
TLC	Thin layer chromatography

Data availability

The supplementary information (SI) is available for readers in the SI which includes ^{1}H NMR, ^{13}C NMR, ^{19}F NMR and mass spectra of the synthesized compounds. Supplementary information is available. See DOI: https://doi.org/10.1039/d6ra02823c.

Acknowledgements

S. Agarwal and S. Teli acknowledge DST-ANRF, SURE (No. SUR/2022/001312) for the financial support. S. Agarwal also sincerely acknowledges Ministry of Education, SPD-RUSA Rajasthan for providing NMR facility under RUSA 2.0, Research and Innovation project (file no./RUSA/GEN/MLSU/2020/6394). The authors are thankful to Department of Chemistry, MLSU, Udaipur for providing research facilities. They are also thankful to IIT Jammu, SAIF-Chandigarh, Department of Physics for analyzing HRMS, HRTEM, UV-vis, fluorescence, EDX, and XRD respectively.

References

1 A. Dandia, P. Saini, M. Sethi, K. Kumar, S. Saini, S. Meena, S. Meena and V. Parewa, Nanocarbons in quantum regime: An emerging sustainable catalytic platform for organic synthesis, *Catal. Rev.*, 2023, **65**(3), 874–928.

2 S. Saini, K. Kumar, P. Saini, D. K. Mahawar, K. S. Rathore, S. Kumar, A. Dandia and V. Parewa, Sustainable synthesis of biomass-derived carbon quantum dots and their catalytic application for the assessment of α, β-unsaturated compounds, *RSC Adv.*, 2022, **12**(50), 32619–32629.

3 T. Yue, J.-B. Wang, X.-Y. Wang, M.-Y. Huang, M. Zhang and Z.-H. Zhang, Metal-free carbon quantum dots as photocatalyst for phosphonation of undirected heteroaryl compounds, *Chin. Chem. Lett.*, 2025, 112050.

4 R. Manjupriya and S. M. Roopan, Carbon dots-based catalyst for various organic transformations, *J. Mater. Sci.*, 2021, **56**(31), 17369–17410.

5 B. Thangaraj, P. R. Solomon, S. Chuangchote, N. Wongyao and W. Surareungchai, Biomass-derived carbon quantum dots–A review. Part 1: Preparation and characterization, *ChemBioEng Rev.*, 2021, **8**(4), 265–301.

6 V. Sindhia and R. Bairwa, Plant review: *Butea monosperma*, *Int. J. Pharm. Chem. Res.*, 2010, **2**(2), 90–94.

7 A. P. Taylor, R. P. Robinson, Y. M. Fobian, D. C. Blakemore, L. H. Jones and O. Fadeyi, Modern advances in heterocyclic chemistry in drug discovery, *Org. Biomol. Chem.*, 2016, **14**(28), 6611–6637.

8 A. K. Tiwari and M. V. Singh, Insights into the origin and therapeutic implications of benzopyran and its derivatives, *ChemistrySelect*, 2023, **8**(20), e202300220.

9 J. Mori, M. Iwashima, M. Takeuchi and H. Saito, A synthetic study on antiviral and antioxidative chromene derivative, *Chem. Pharm. Bull.*, 2006, **54**(3), 391–396.

10 S. Thareja, A. Verma, A. Kalra, S. Gosain, P. V. Rewatkar and G. R. Kokil, Novel chromeneimidazole derivatives as antifungal compounds: Synthesis and in vitro evaluation, *Acta Pol. Pharm.*, 2010, **67**, 423–427.

11 C. B. Sangani, N. M. Shah, M. P. Patel and R. G. Patel, Microwave assisted synthesis of novel 4*H*-chromene derivatives bearing phenoxypyrazole and their antimicrobial activity assess, *J. Serb. Chem. Soc.*, 2012, **77**(9), 1165–1174.

12 N. R. Kamdar, D. D. Haveliwala, P. T. Mistry and S. K. Patel, Synthesis and evaluation of in vitro antitubercular activity and antimicrobial activity of some novel 4*H*-chromeno [2, 3-d] pyrimidine via 2-amino-4-phenyl-4*H*-chromene-3-carbonitriles, *Med. Chem. Res.*, 2011, **20**(7), 854–864.

13 B. Musicki, A.-M. Periers, P. Laurin, D. Ferroud, Y. Benedetti, S. Lachaud, F. Chatreaux, J.-L. Haesslein, A. Iltis and C. Pierre, Improved antibacterial activities of coumarin antibiotics bearing 5′, 5′-dialkylnoviose: biological activity of RU79115, *Bioorg. Med. Chem. Lett.*, 2000, **10**(15), 1695–1699.

14 A. Yasmin, A. Passi, R. Jha, P. Saha, K. Sharma, S. Jindal and K. Goyal, Benzopyran derivatives as emerging anticancer agents: Advances in synthesis, SAR insights, and therapeutic potential, *ChemistrySelect*, 2025, **10**(35), e02424.

15 S. Gupta, N. Kumar, S. Kumar, R. Dudhe and P. Sharma, 3-Hydroxy-2-(substituted phenyl)-4*H*-chromen-4-one derivatives-synthesis, spectral characterization and pharmacological screening, *Int. J. Theor. Appl.*, 2012, **7**, 1–8.

16 G. Megha and Y. D. Bodke, Synthesis of 7-{[2-(4-substituted phenyl)-2-oxoethyl] amino}-4-methyl-2*H*-1-benzopyran-2-one derivatives and evaluation of their pharmacological activities, *ChemistrySelect*, 2024, **9**(5), e202303421.

17 O. M. Abdelhafez, K. M. Amin, R. Z. Batran, T. J. Maher, S. A. Nada and S. Sethumadhavan, Synthesis, anticoagulant and PIVKA-II induced by new 4-hydroxycoumarin derivatives, *Bioorg. Med. Chem.*, 2010, **18**(10), 3371–3378.

18 M. A. Bhat, N. Siddiqui and S. A. Khan, Synthesis of novel 3-(4-acetyl-5*H*/methyl-5-substituted phenyl-4, 5-dihydro-1, 3, 4-oxadiazol-2-yl)-2*H*-chromen-2-ones as potential anticonvulsant agents, *Acta Pol. Pharm.*, 2008, **65**(2), 235–239.

19 Y. Kang, Y. Mei, Y. Du and Z. Jin, Total synthesis of the highly potent anti-HIV natural product daurichromenic acid along with its two chromane derivatives, rhododaurichromanic acids A and B, *Org. Lett.*, 2003, **5**(23), 4481–4484.

20 S.-S. Zhang, W.-H. Liu, Z.-W. He, Q.-W. Tan and L.-P. Guan, Synthesis of chromen-1-phenylpropan-1-one derivatives and their antidepressant/anticonvulsant activities, *Lett. Drug Des. Discovery*, 2021, **18**(12), 1136–1145.

21 L. Saher, M. Makhloufi-Chebli, L. Dermeche, S. Dermeche, B. Boutemeur-Khedis, C. Rabia, M. Hamdi and A. M. Silva, 10-(4-Hydroxy-6-methyl-2-oxo-2*H*-pyran-3-yl)-3-methyl-1*H*, 10*H*-pyrano [4, 3-*b*] chromen-1-ones from a pseudo-multicomponent reaction and evaluation of their antioxidant activity, *Tetrahedron*, 2018, **74**(8), 872–879.

22 M. N. Elinson, S. V. Gorbunov, A. N. Vereshchagin, R. F. Nasybullin, A. S. Goloveshkin, I. S. Bushmarinov and M. P. Egorov, Chemical and electrocatalytic cascade

cyclization of salicylaldehyde with three molecules of malononitrile:'One-pot'simple and efficient way to the chromeno [2, 3-*b*] pyridine scaffold, *Tetrahedron*, 2014, **70**(45), 8559–8563.

23 R. Sangsuwan, S. Sangher, T. Aree, C. Mahidol, S. Ruchirawat and P. Kittakoop, An organocatalyst from renewable materials for the synthesis of coumarins and chromenes: Three-component reaction and multigram scale synthesis, *RSC Adv.*, 2014, **4**(26), 13708–13718.

24 S. S. Acharya, L. M. Barad, P. R. Rout, A. Bisoyi and B. B. Parida, Ultrasonication-assisted multicomponent green and sustainable synthesis of benzopyrans employing taurine as a bioorganic catalyst, *New J. Chem.*, 2025, **49**(28), 12090–12101.

25 M. Tajbakhsh, M. Heidary and R. Hosseinzadeh, Nano Fe/NaY zeolite: An efficient and reusable solid-supported catalyst for synthesis of 1-oxo-hexahydroxanthene and tetraketone derivatives, *Res. Chem. Intermed.*, 2016, **42**(2), 1425–1439.

26 B. S. Kuarm, J. V. Madhav, S. V. Laxmi, B. Rajitha, Y. T. Reddy, P. N. Reddy and P. A. Crooks, Cellulose sulfuric acid: An efficient biodegradable and recyclable solid acid catalyst for the synthesis of 1-oxo-hexahydroxanthene, *Synth. Commun.*, 2011, **41**(12), 1719–1724.

27 T. R. Mandlimath, B. Umamahesh and K. I. Sathiyanarayanan, Rapid one pot synthesis of xanthene derivatives by an efficient and reusable nano-$ZnAl_2O_4$–An insight into a new process, *J. Mol. Catal. A: Chem.*, 2014, **391**, 198–207.

28 N. Sato, M. Jitsuoka, T. Shibata, T. Hirohashi, K. Nonoshita, M. Moriya, Y. Haga, A. Sakuraba, M. Ando and T. Ohe, (9S)-9-(2-Hydroxy-4, 4-dimethyl-6-oxo-1-cyclohexen-1-yl)-3, 3-dimethyl-2, 3, 4, 9-tetrahydro-1*H*-xanthen-1-one, a selective and orally active neuropeptide Y Y5 receptor antagonist, *J. Med. Chem.*, 2008, **51**(15), 4765–4770.

29 M. M. Heravi, P. Ansari, M. Saeedi, N. Tavakoli-Hosseini and N. Karimi, Green and practical synthesis of benzopyran and 3-sunstituted coumarin derivatives by Brønsted acid ionic liquid $[(CH_2)_4SO_3HMIM][HSO_4]$, *Bull. Chem. Soc. Ethiop.*, 2011, **25**(2), 315–320.

30 S. R. Kamat, A. H. Mane, A. D. Patil, T. R. Lohar and R. S. Salunkhe, Synthesis of xanthene and coumarin derivatives in water by using β-cyclodextrin, *Res. Chem. Intermed.*, 2021, **47**(3), 911–924.

31 S. T. Morbale, S. D. Jadhav, M. B. Deshmukh and S. S. Patil, Bronsted acid-type biosurfactant for heterocyclization: A green protocol for benzopyran synthesis, *RSC Adv.*, 2015, **5**(103), 84610–84620.

32 S. M. Snehali Mali, S. S. Sachin Shinde, S. D. Shashikant Damte and S. P. Suresh Patil, Synergistic effect of natural chickpea leaf exudates acids in heterocyclization: A greener protocol for benzopyran synthesis, *R. Soc. Open Sci.*, 2018, **5**(2), 170333.

33 R. Chugh and G. Kaur, Citrus limetta peels derived carbon dots as highly active carbocatalyst for carbon–carbon bond formation, *Clean Technol. Environ. Policy*, 2024, **26**(11), 3907–3919.

34 R. B. Rotti, S. Shafi, G. Nagaraju, G. M. Gouda, D. Sunitha and G. Darshan, Design and synthesis of quasi-spherical fluorescent carbon quantum dots for visualization of latent fingerprints, *J. Mol. Struct.*, 2025, **1333**, 141674.

35 K. Kasinathan, S. Samayanan, K. Marimuthu and J.-H. Yim, Green synthesis of multicolour fluorescence carbon quantum dots from sugarcane waste: Investigation of mercury (II) ion sensing, and bio-imaging applications, *Appl. Surf. Sci.*, 2022, **601**, 154266.

36 A. Mohammadi, N. Haghnazari and C. Karami, Nano-probe for determination of phenobarbital of green synthesized fluorescent carbon dots using *Scrophularia striata*, *J. Mater. Sci.: Mater. Electron.*, 2023, **34**(4), 251.

37 N. G. Alamdari, H. Almasi, M. Moradi and M. Akhgari, Characterization of carbon quantum dots synthesized from vinasse and date seeds as agro-industrial wastes, *Waste Biomass Valorization*, 2023, **14**(11), 3689–3703.

38 A. Dager, T. Uchida, T. Maekawa and M. Tachibana, Synthesis and characterization of mono-disperse carbon quantum dots from fennel seeds: Photoluminescence analysis using machine learning, *Sci. Rep.*, 2019, **9**(1), 14004.

39 K. Dehvari, K. Y. Liu, P.-J. Tseng, G. Gedda, W. M. Girma and J.-Y. Chang, Sonochemical-assisted green synthesis of nitrogen-doped carbon dots from crab shell as targeted nanoprobes for cell imaging, *J. Taiwan Inst. Chem. Eng.*, 2019, **95**, 495–503.

40 R. Purbia and S. Paria, A simple turn on fluorescent sensor for the selective detection of thiamine using coconut water derived luminescent carbon dots, *Biosens. Bioelectron.*, 2016, **79**, 467–475.

41 N. Sudhan, K. Subramani, M. Karnan, N. Ilayaraja and M. Sathish, Biomass-derived activated porous carbon from rice straw for a high-energy symmetric supercapacitor in aqueous and non-aqueous electrolytes, *Energy Fuels*, 2017, **31**(1), 977–985.

42 C. Zequine, C. Ranaweera, Z. Wang, S. Singh, P. Tripathi, O. Srivastava, B. K. Gupta, K. Ramasamy, P. Kahol and P. Dvornic, High performance and flexible supercapacitors based on carbonized bamboo fibers for wide temperature applications, *Sci. Rep.*, 2016, **6**(1), 31704.

43 S. Kumawat, D. K. Meena, M. Rani, H. S. Mund and G. Arora, Effect of Mg doping at Fe/Cr site on magnetic and optical properties of Gd_2FeCrO_6 double perovskite, *J. Alloys Compd.*, 2024, **978**, 173339.

44 H. Nie, M. Li, Q. Li, S. Liang, Y. Tan, L. Sheng, W. Shi and S. X.-A. Zhang, Carbon dots with continuously tunable full-color emission and their application in ratiometric pH sensing, *Chem. Mater.*, 2014, **26**(10), 3104–3112.

45 S. Ding, Y. Gao, B. Ni and X. Yang, Green synthesis of biomass-derived carbon quantum dots as fluorescent probe for Fe^{3+} detection, *Inorg. Chem. Commun.*, 2021, **130**, 108636.

46 S. Teli, S. Soni, N. Rana, A. Manhas and S. Agarwal, From botanical waste to a biocatalyst: *Kigelia pinnata* flower-

derived CQDs for triazolidine-3-thione synthesis and their in silico evaluation, *Nanoscale Adv.*, 2025, **7**(24), 8104–8121.
47 D. Prasad, A. Preetam and M. Nath, L-Proline-accelerated, eco-friendly synthesis of 9-substituted-2, 3, 4, 9-tetrahydro-1*H*-xanthen-1-ones under mild conditions, *C. R. Chim.*, 2013, **16**(12), 1153–1157.
48 D. Pore, T. Shaikh, K. Undale and D. Gaikwad, A green protocol for catalyst-free synthesis of 1-oxo-hexahydroxanthenes in aqueous medium, *C. R. Chim.*, 2010, **13**(12), 1429–1432.
49 T. Lohar, A. Mane, S. Kamat, A. Kumbhar and R. Salunkhe, Trifluoroethanol and liquid-assisted grinding method: A green catalytic access for multicomponent synthesis, *Res. Chem. Intermed.*, 2018, **44**(3), 1919–1933.
50 X.-S. Wang, Z.-S. Zeng, M.-M. Zhang, D.-Q. Shi and S.-J. Tu, Unexpected ring-opening of a 2-pyrone ring in the synthesis of 3-[(Z)-1-hydroxy-3-oxobut-1enyl]-2*H*-chromen-2-one derivatives catalysed by Kf-Alumina, *J. Chem. Res.*, 2006, **2006**(9), 602–604.
51 M. Zhang, M. N. Chen and Z. H. Zhang, Visible light-initiated catalyst-free one-pot, multicomponent construction of 5-substituted indole chromeno [2, 3-*b*] pyridines, *Adv. Synth. Catal.*, 2019, **361**(22), 5182–5190.
52 A. Lapkin and D. Constable, *Green Chemistry Metrics: Measuring and Monitoring Sustainable Processes*, Wiley, Chichester, 2008.
53 J. Martínez, J. F. Cortés and R. Miranda, Green chemistry metrics, a review, *Processes*, 2022, **10**(7), 1274.
54 https://www.way2drug.com/PassOnline/.
55 Y. Ogino, N. Ohtake, Y. Nagae, K. Matsuda, M. Moriya, T. Suga, M. Ishikawa, M. Kanesaka, Y. Mitobe and J. Ito, Design, syntheses, and structure–activity relationships of novel NPY Y5 receptor antagonists: 2-{3-Oxospiro [isobenzofuran-1 (3*H*), 4′-piperidin]-1′-yl} benzimidazole derivatives, *Bioorg. Med. Chem. Lett.*, 2008, **18**(18), 5010–5014.
56 M. Fichtner, E. Lee, E. Tomlinson, D. Scott, P. Cornelius, T. A. Patterson and P. A. Carpino, Discovery and evaluation of spirocyclic derivatives as antagonists of the neuropeptide Y5 receptor, *Bioorg. Med. Chem. Lett.*, 2012, **22**(8), 2738–2743.
57 H. Domin and Y. Neuropeptide, Y2 and Y5 receptors as potential targets for neuroprotective and antidepressant therapies: Evidence from preclinical studies, *Prog. Neuro-Psychopharmacol. Biol. Psychiatry*, 2021, **111**, 110349.
58 F. M. Ferguson and N. S. Gray, Kinase inhibitors: The road ahead, *Nat. Rev. Drug Discovery*, 2018, **17**(5), 353–377.
59 T. Tang, C. Hartig, Q. Chen, W. Zhao, A. Kaiser, X. Zhang, H. Zhang, H. Qu, C. Yi and L. Ma, Structural basis for ligand recognition of the neuropeptide Y Y2 receptor, *Nat. Commun.*, 2021, **12**(1), 737.
60 B. Xu, H. Fallmar, L. Boukharta, J. Pruner, I. Lundell, N. Mohell, H. Gutierrez-de-Teran, J. Åqvist and D. Larhammar, Mutagenesis and computational modeling of human G-protein-coupled receptor Y2 for neuropeptide Y and peptide YY, *Biochemistry*, 2013, **52**(45), 7987–7998.
61 R. Y. Patel and R. J. Doerksen, Protein kinase− inhibitor database: Structural variability of and inhibitor interactions with the protein kinase P-loop, *J. Proteome Res.*, 2010, **9**(9), 4433–4442.
62 https://www2.rcsb.org/.
63 A. J. Liedtke, A. O. Adeniji, M. Chen, M. C. Byrns, Y. Jin, D. W. Christianson, L. J. Marnett and T. M. Penning, Development of potent and selective indomethacin analogues for the inhibition of AKR1C3 (type 5 17β-hydroxysteroid dehydrogenase/prostaglandin F synthase) in castrate-resistant prostate cancer, *J. Med. Chem.*, 2013, **56**(6), 2429–2446.
64 Z. Wang, B. J. Canagarajah, J. C. Boehm, S. Kassisà, M. H. Cobb, P. R. Young, S. Abdel-Meguid, J. L. Adams and E. J. Goldsmith, Structural basis of inhibitor selectivity in MAP kinases, *Structure*, 1998, **6**(9), 1117–1128.
65 Y. Cheng and H. Tian, Current development status of MEK inhibitors, *Molecules*, 2017, **22**(10), 1551.
66 S. Soni, S. Teli, P. Teli, A. Manhas, P. C. Jha and S. Agarwal, Highly efficient synthesis of isoxazolones and pyrazolones using g-C_3N_4·OH nanocomposite with their in silico molecular docking, pharmacokinetics and simulation studies, *Sci. Rep.*, 2024, **14**(1), 19123.
67 S. Thulasi, A. Kathiravan and M. Asha Jhonsi, Fluorescent carbon dots derived from vehicle exhaust soot and sensing of tartrazine in soft drinks, *ACS Omega*, 2020, **5**(12), 7025–7031.
68 C. Zapata-Hernandez, G. Durango-Giraldo, M. Gomez-Echeverri, R. Buitrago-Sierra, B. Herrera and K. Cacua, The impact of carbon quantum dots derived from spent coffee grounds on the droplet combustion of diesel/n-butanol blend, *Heliyon*, 2024, **10**(21), e39671.
69 P. W. Rose, A. Prlić, A. Altunkaya, C. Bi, A. R. Bradley, C. H. Christie, L. D. Costanzo, J. M. Duarte, S. Dutta and Z. Feng, The RCSB protein data bank: Integrative view of protein, gene and 3D structural information, *Nucleic Acids Res.*, 2016, gkw1000.
70 M. Aziz, S. A. Ejaz, H. M. Rehman, A. S. Alsubaie, K. Mahmoud, F. Siddique, M. Al-Buriahi and Z. Alrowaili, Identification of NEK7 inhibitors: Structure based virtual screening, molecular docking, density functional theory calculations and molecular dynamics simulations, *J. Biomol. Struct. Dyn.*, 2023, **41**(14), 6894–6908.
71 M. Rarey, B. Kramer, T. Lengauer and G. Klebe, A fast flexible docking method using an incremental construction algorithm, *J. Mol. Biol.*, 1996, **261**(3), 470–489.
72 N. M. O'Boyle, M. Banck, C. A. James, C. Morley, T. Vandermeersch and G. R. Hutchison, Open Babel: An open chemical toolbox, *J. Cheminf.*, 2011, **3**(1), 33.
73 D. E. Pires, T. L. Blundell and D. B. Ascher, pkCSM: predicting small-molecule pharmacokinetic and toxicity properties using graph-based signatures, *J. Med. Chem.*, 2015, **58**(9), 4066–4072.
74 S. S. Acharya, L. M. Barad, P. R. Rout, A. Bisoyi and B. B. Parida, Ultrasonication-assisted, multicomponent, green and sustainable synthesis of benzopyrans employing

taurine as a bioorganic catalyst, *New J. Chem.*, 2025, **49**(28), 12090–12101.

75 M. Snehali, S. Sachin, D. Shashikant and P. Suresh, Synergistic effect of natural chickpea leaf exudates acids in heterocyclization: A greener protocol for benzopyran synthesis, *R. Soc. Open Sci.*, 2018, **5**(2), 17033.

76 L. Kamilia Ould, M.-C. Malika, B.-T. Amina, T.-B. Souhila, H. Nejla, M. S. S. Artur and B. Jean-Bernard, Selectivity control in the reaction between 2-hydroxyarylaldehydes and 4-hydroxycoumarin. Antioxidant activities and computational studies of the formed products, *J. Mol. Struct.*, 2021, **1231**, 129936.

77 S. Abdolmohammadi, H. Pirelahi, F. Balalaie and S. Balalaie, Efficient synthesis of dihydrochromeno [4, 3-*b*] chromenone and derivatives in aqueous media, *Heterocycl. Commun.*, 2010, **16**(1), 13–20.

78 S. R. Kamat, R. S. Salunkhe, P. B. Choudhari, R. P. Dhavale, A. H. Mane and T. R. Lohar, Efficient synthesis of chromeno [2, 3-*c*] pyrazolyl-pyrazolol (*s*) in hydrotropic solution and their anti-infective potential, *Res. Chem. Intermed.*, 2018, **44**(2), 1351–1362.

79 N. E. Michail, V. G. Sergey, N. V. Anatoly, F. N. Ruslan, S. G. Alexander, S. B. Ivan and P. E. Mikhail, Chemical and electrocatalytic cascade cyclization of salicylaldehyde with three molecules of malononitrile: 'One-pot' simple and efficient way to the chromeno 2,3-*b* pyridine scaffold, *Tetrahedron*, 2014, **70**(45), 8559–8563.